

DOT/FAA/AR-11/14

Federal Aviation Administration
William J. Hughes Technical Center
Aviation Research Division
Atlantic City International Airport
New Jersey 08405

Probabilistic Structural Risk Assessment and Risk Management for Small Airplanes

November 2017

Final Report

This document is available to the U.S. public through the National Technical Information Services (NTIS), Springfield, Virginia 22161.

This document is also available from the Federal Aviation Administration William J. Hughes Technical Center at actlibrary.tc.faa.gov.



U.S. Department of Transportation
Federal Aviation Administration

NOTICE

This document is disseminated under the sponsorship of the U.S. Department of Transportation in the interest of information exchange. The U.S. Government assumes no liability for the contents or use thereof. The U.S. Government does not endorse products or manufacturers. Trade or manufacturers' names appear herein solely because they are considered essential to the objective of this report. The findings and conclusions in this report are those of the author(s) and do not necessarily represent the views of the funding agency. This document does not constitute FAA policy. Consult the FAA sponsoring organization listed on the Technical Documentation page as to its use.

This report is available at the Federal Aviation Administration William J. Hughes Technical Center's Full-Text Technical Reports page: actlibrary.tc.faa.gov in Adobe Acrobat portable document format (PDF).

1. Report No. DOT/FAA/AR-11/14		2. Government Accession No.		3. Recipient's Catalog No.	
4. Title and Subtitle PROBABILISTIC STRUCTURAL RISK ASSESSMENT AND RISK MANAGEMENT FOR SMALL AIRPLANES				5. Report Date November 2017	
				6. Performing Organization Code	
7. Author(s) Harry Millwater, Juan Ocampo, Gulshan Singh, Herb Smith, and Eric Meyer				8. Performing Organization Report No.	
9. Performing Organization Name and Address				10. Work Unit No. (TRAVIS)	
				11. Contract or Grant No.	
12. Sponsoring Agency Name and Address U.S. Department of Transportation Federal Aviation Administration FAA Central Regional Office 901 Locust St Kansas City, MO 64106				13. Type of Report and Period Covered	
				14. Sponsoring Agency Code ACE-113	
15. Supplementary Notes The FAA William J. Hughes Technical Center Aviation Research Division Technical Monitor was Dr. Sohrob Mottaghi.					
16. Abstract A risk assessment evaluation of the continued operational safety of general aviation (GA) fleet can provide important insight to the criticality/severity of a potentially serious structural issue. As such, the methodology to address risk assessment and risk management of GA structural issues was developed. This information will provide a proactive approach to enable a nonbiased review of data to assure airworthiness. The methodology considers the random variables					
17. Key Words Miner's rule, probabilistic safe-life			18. Distribution Statement This document is available to the U.S. public through the National Technical Information Service (NTIS), Springfield, Virginia 22161.		
19. Security Classif. (of this report) Unclassified		20. Security Classif. (of this page) Unclassified		21. No. of Pages 50	22. Price

ACKNOWLEDGEMENTS

The authors would like to acknowledge the significant help provided by Carlos Acosta for computer implementation of the probabilistic algorithms during internships (2009 & 2010), and Dr. K. Raju (Wichita State Univeristy) for providing the experimental data and insightful discussions throughout the duration of the project.

TABLE OF CONTENTS

	Page
EXECUTIVE SUMMARY	viii
1. INTRODUCTION	1
2. METHODOLOGY	1
2.1 Overview	4
2.2 Random variables	4
2.2.1 Gust and Maneuver Loads	5
2.2.2 Sink Rate	11
2.2.3 Flight Velocity-Duration	15
2.2.4 Flight Weight-Duration	17
2.2.5 Probabilistic Stress Life	17
2.2.6 Stress Severity Factor	23
2.2.7 Miner's damage index	26
2.3 Numerical Examples	31
2.3.1 Damage Mode	33
2.3.2 Hours Mode	37
3. CONCLUSIONS	38
4. REFERENCES	39

LIST OF FIGURES

Figure		Page
1	Schematic of risk assessment methodology for the spectrum generation	2
2	Schematic of risk assessment methodology for the damage accumulation	3
3	Schematic of risk assessment methodology for damage accumulation	4
4	Random maneuver schematic data	7
5	Random gust/maneuver generation flowchart	9
6	Random gust confidence bounds	10
7	Random gust data generation	11
8	Landing impact spectra	12
9	Sink rate probability distribution function	14
10	Sink rate CDF	14
11	Flight length and airspeed joint PDF	16
12	Hi-Lok fastener 6 KSI mean stress 30% load transfer	20
13	Open hole 3 KSI mean stress	20
14	Open hole 3 KSI mean stress	21
15	Open hole 6 KSI mean stress	22
16	Hi-Lok fastener 6 KSI mean stress 50% load transfer	22
17	Load fastener, load transfer, and bypass load	23
18	Hi-Lok 30% load transfer 3 KSI mean stress	24
19	S-N prediction using OH data and SSF	26
20	Random miner's stress spectrum flowchart	27
21	Random Miner's damage index accumulation flowchart	28
22	PDF normal usage, high severity, and OH	29
23	PDF aerobatic usage, high severity, and OH	30
24	PDF normal usage, low severity, and OH	30
25	Flight length and flight velocity joint PDF for instructional usage	32
26	Flight length and flight velocity joint PDF for personal usage	33
27	Flights-to-failure probability plot testing	35
28	Flights-to-failure PDF	36
29	Hours-to-failure PDF	36
30	Mean damage results	38

LIST OF TABLES

Table		Page
1	Code variable classification	1
2	Probabilistic usage groups	5
3	Statistical data for positive maneuver	6
4	Example calculation of statistical data	8
5	Sink rate CDF construction	13
6	Flight length and airspeed data	15
7	Flight length and airspeed joint PDF	16
8	Flight length and airspeed conditionals	17
9	Data available to develop P-S-N curves [2,3]	18
10	Random damage index summary results	29
11	Flight length and airspeed data for instructional usage	31
12	Flight length and airspeed data for personal usage	32
13	Flight length and weight data for instructional and personal usage	33
14	Analysis data	34
15	Safe-life analysis results	35
16	Correlation analysis personal and instructional usage	37
17	Correlation analysis instructional usage	37
18	Correlation analysis personal usage	37
19	Probability-of-failure results	38

LIST OF ACRONYMS

CB	Confidence bounds
CDF	Cumulative distribution function
COV	Coefficient of variation
FH	Filled hole
MPI	Message Passing Interface
OH	Open hole
OpenMP	Open Multi-Processing
PDF	Probability density function
POF	Probability-of-failure
P-S-N	Probabilistic stress-life
S-N	Stress-life
SSF	Stress severity factor

EXECUTIVE SUMMARY

Probabilistic fatigue evaluation of General Aviation aircraft is vital to provide important insight into the severity or criticality of a potential structural issue. In this report, a probabilistic risk assessment methodology is developed for risk assessment and risk management of structural-fatigue-failure issues. Because of significant airplane-to-airplane and flight-to-flight variations, probability density functions of the critical variables were investigated and developed. The methodology developed in this report is incorporated into the SMART (Small Aircraft Risk Technology) software, which has been developed under FAA support. Moreover, the methodology and software were demonstrated on two different structural risk-assessment examples.

1. INTRODUCTION

In 1991, Congress mandated that the FAA establish an Aging Aircraft Program. The focus of this program was age-related structural problems with airplanes used in public transportation. At the time, Congress excluded the GA fleet from the mandate. However, the FAA determined that, as the GA fleet continues to age, there is concern about ensuring the continued airworthiness of the diverse GA fleet. To guide future efforts in addressing the effects of aging on GA airplanes, the Small Airplane Directorate developed an FAA Aging GA Roadmap that serves as a guide to proactively manage the overall airworthiness of aging GA airplanes. One of the four major focus areas of the roadmap is data-driven risk assessment and risk management. As a result, a research and development program was undertaken to develop the required methodology, computer software, and supporting data to conduct structural risk assessments.

2. METHODOLOGY

The methodology in this work encompasses the required elements necessary to conduct a structural integrity evaluation and considers real-world airplane-to-airplane and flight-to-flight variations such that a realistic risk assessment of an aircraft structural detail can be performed. Table 1 shows a summary of the variables used to conduct the risk assessment.

Table 1. Code variable classification

Variable	Type
Gust/Maneuver Load Exceedances	Probabilistic: (Lognormal) [1]
Aircraft Velocity and Flight Duration	Probabilistic: (joint pdf with correlated variables)
Sink Rate	Probabilistic
Damage Index	Probabilistic: (normal or Weibull distribution)
Maneuver Load Limit Factors	Deterministic
Gust Load Limit Factors	Deterministic
Ground Stress	Probabilistic: (joint pdf with correlated variables)
One-g Stress	Probabilistic: (joint pdf with correlated variables)
P-S-N	Probabilistic (determined from regression modeling of constant amplitude tests) [2,3]
Miner's Damage Index	Probabilistic (Weibull or Normal – fit to variable amplitude tests) [2,3]

P-S-N = probabilistic stress-life

To perform a risk evaluation, two different methodologies that follow the FAA guidelines used for safe-life evaluation (i.e., AFS-120-73[4] and Advisory Circular (AC) 23-13A[5]) were incorporated in a computer code. The first methodology calculates the flights and hours-to-failure (or the safe-life) time to crack initiation for GA. This methodology is explained step by step as follows:

- Variables such as airplane usage, load limit factors, ground stress, one-g stress, airplane velocity, and flight length are input by the user.
- According to the airplane usage (e.g., single-engine unpressurized instructional, pressurized usage, twin-engine general usage), the respective data (exceedance curves, sink rate data, etc.) are loaded from internal libraries.
- Realizations of the random variables (e.g., sink rate velocity, airplane velocity, and flight duration) needed for Monte Carlo sampling are generated. A weighted mix of usages is allowed.
- For each Monte Carlo sample, the code generates a characteristic stress spectrum that includes the flight stages: gust, maneuver, taxi, ground-air-ground, and landing and rebound. The methodology process through this point is shown in figure 1.
- Damage is accumulated for each Monte Carlo sample using Miner's rule until Miner's critical value (damage index) is reached, and the flights/hours-to-failure are recorded (see figure 2).
- When the Monte Carlo sampling is finished, the random variables and flights/hours-to-failure are post-processed to determine the distribution of flights/hours-to-failure (e.g., probabilities, mean, standard deviation, confidence intervals, and hazard function) and to identify the significant random variables using correlation coefficients.

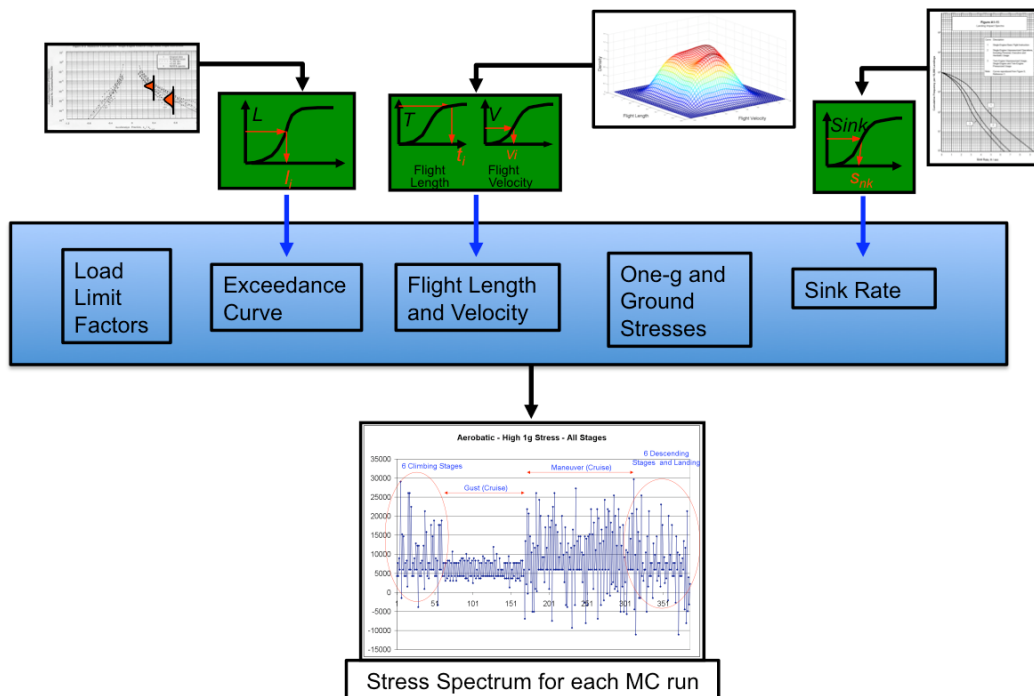


Figure 1. Schematic of risk assessment methodology for the spectrum generation

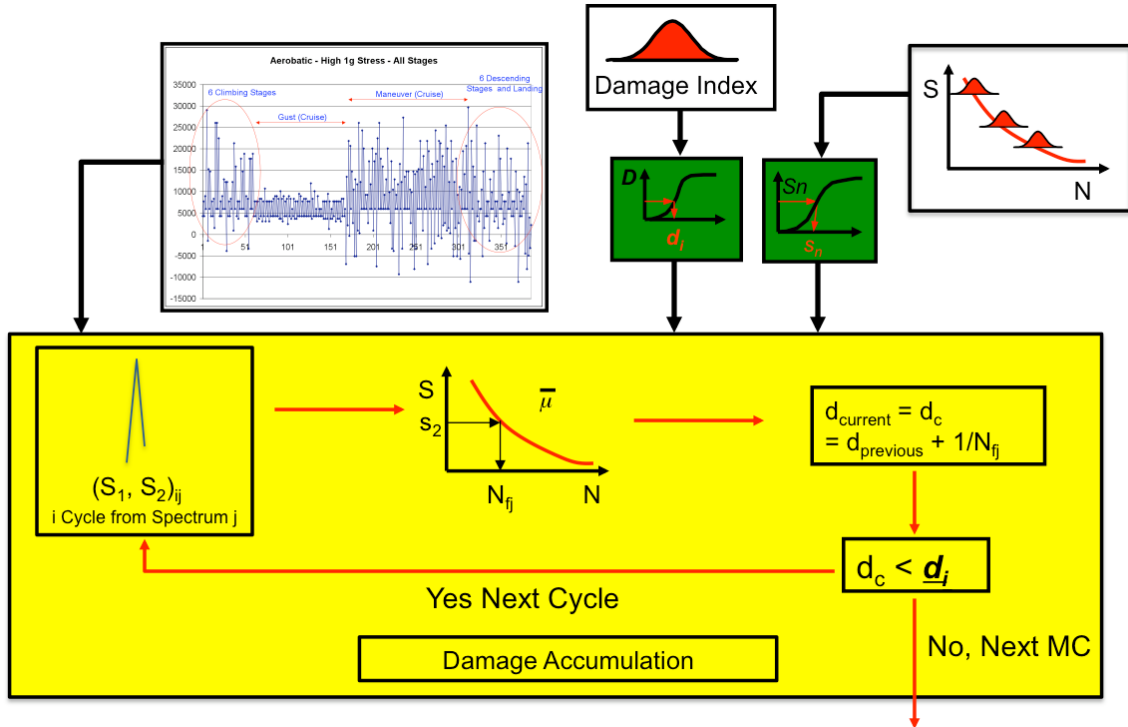


Figure 2. Schematic of risk assessment methodology for the damage accumulation

The second methodology calculates the accumulated damage condition and the probability-of-failure (POF), given any number of hours flown by the airplane. The methodology is explained as follows:

- The same steps shown for the first methodology to generate the stress spectrum are used in this methodology (see figure 1).
- Damage is accumulated for each Monte Carlo sample until the flight hours specified by the user are reached. The accumulated damage is recorded, as shown in figure 3.
- If the damage recorded is larger than the random Miner's damage coefficient generated for that sample, a failure is counted.
- When the Monte Carlo sampling is finished, the random variables, the accumulated damage, and the failures are post-processed to obtain the POF, percentage damage per flight stage, and the significant random variables.

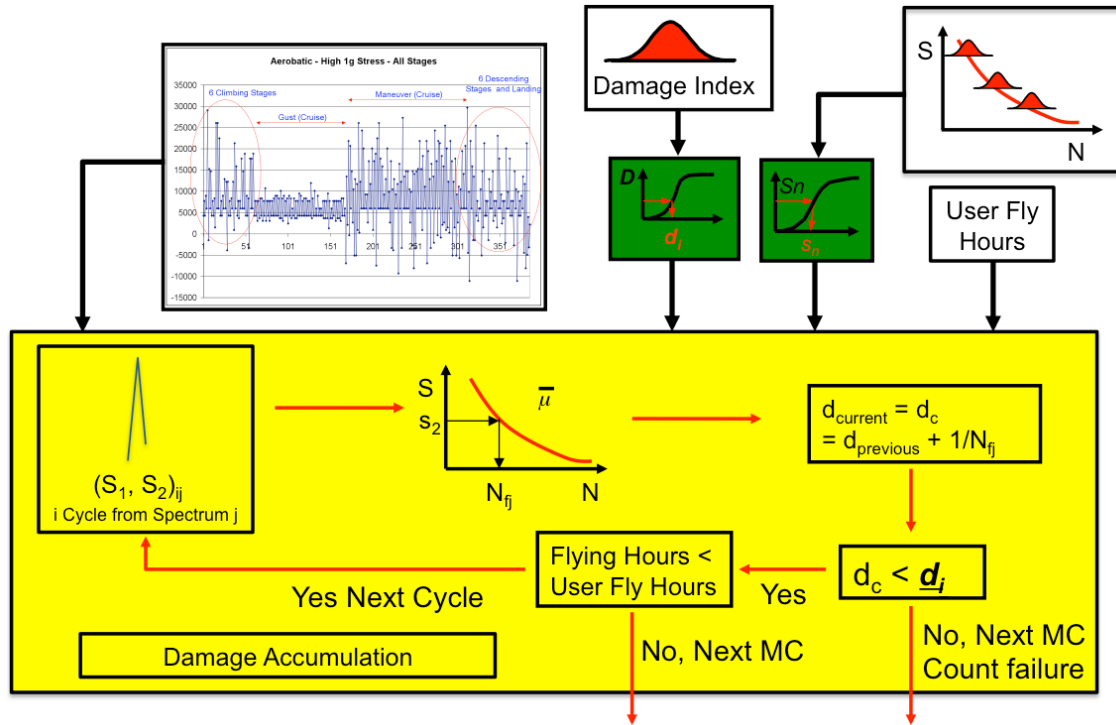


Figure 3. Schematic of risk assessment methodology for damage accumulation

Given the significant airplane-to-airplane and flight-to-flight variations, an essential ingredient of the methodology was to investigate, develop, and model probability density functions (PDFs) of the critical input data, such as flight duration, aircraft speed, sink rate velocity, and the damage index coefficient. Probabilistic stress-life (P-S-N) curves are being developed using data from an experimental program conducted by Wichita State University under a separate program [2, 3].

Sensitivity analysis is an essential ingredient of risk assessment. The Monte Carlo sampling results are post-processed to predict the risk of failure and the associated sensitivities. The sensitivities indicate the relative importance of the inputs on the life estimation. Various sensitivity methods are available, such as scatter plots, segmented PDFs, regression, and others [6].

The Monte Carlo sampling risk assessment methodology is well suited to parallel implementation. Therefore, the Monte Carlo samples were distributed to multiple processors using the Open Multi-Processing (OpenMP) and Message Passing Interface (MPI) parallel methods [7, 8]. Significant speed-ups were obtained for both methods; 6.87 using 8 processors with OpenMP and 312 using 512 processors with MPI.

2.1 OVERVIEW

2.2 RANDOM VARIABLES

An overview of the random variables was presented in table 1. Further details for each random variables are given below.

2.2.1 Gust and Maneuver Loads

To create statistical distributions from the data already recorded in the NASA Velocity-Gs/Velocity-Gs-Altitude [9], Reyer [1] developed lognormal distributions for usages shown in table 2. These distributions of usages are used in the code.

Table 2. Probabilistic usage groups

Usage Group
Single-engine unpressurized usage basic flight instruction
Single-engine unpressurized usage personal usage
Single-engine unpressurized usage executive usage
Single-engine unpressurized usage aerobatic usage
Twin-engine unpressurized usage basic flight instruction
Twin-engine unpressurized usage general
Pressurized usage
Agricultural usage

For this random variable, the code generates a random family of gust and maneuver exceedances for each specific Monte Carlo simulation. An example from the data obtained from Reyer [1] is shown in table 3.

Table 3. Statistical data for positive maneuver

Single-Engine Unpressurized Usage Basic Flight Instruction		
Acceleration Fraction	Mean Frequency (Incremental) per Nautical Mile	COV (% of Mean Frequency)
+0.10	4.89089×10^{-1}	12%
+0.15	1.02496×10^{-1}	12%
+0.20	2.92114×10^{-2}	12%
+0.25	6.42846×10^{-3}	12%
+0.30	1.72636×10^{-3}	12%
+0.35	5.29138×10^{-4}	12%
+0.40	1.75933×10^{-4}	12%
+0.45	6.17108×10^{-5}	12%
+0.50	2.22439×10^{-5}	12%
+0.55	8.13099×10^{-6}	12%
+0.60	2.97563×10^{-6}	12%
+0.65	1.08834×10^{-6}	12%
+0.70	3.97802×10^{-7}	12%
+0.75	1.45412×10^{-7}	12%
+0.80	5.31542×10^{-8}	12%
+0.85	1.94290×10^{-8}	12%
+0.90	7.10186×10^{-9}	12%
+0.95	2.59604×10^{-9}	12%
+1.00	1.57931×10^{-9}	12%

COV = coefficient of variation

In table 3, for each acceleration fraction, information is given for the mean and the coefficient of variation (COV). The COV is a measure of the dispersion of the data relative to the mean. The procedure used to generate random data can be explained as follows:

Figure 4 shows random maneuver data schematically. It is clear that the distributions are created at each acceleration level and that the random data are the frequency of occurrence.

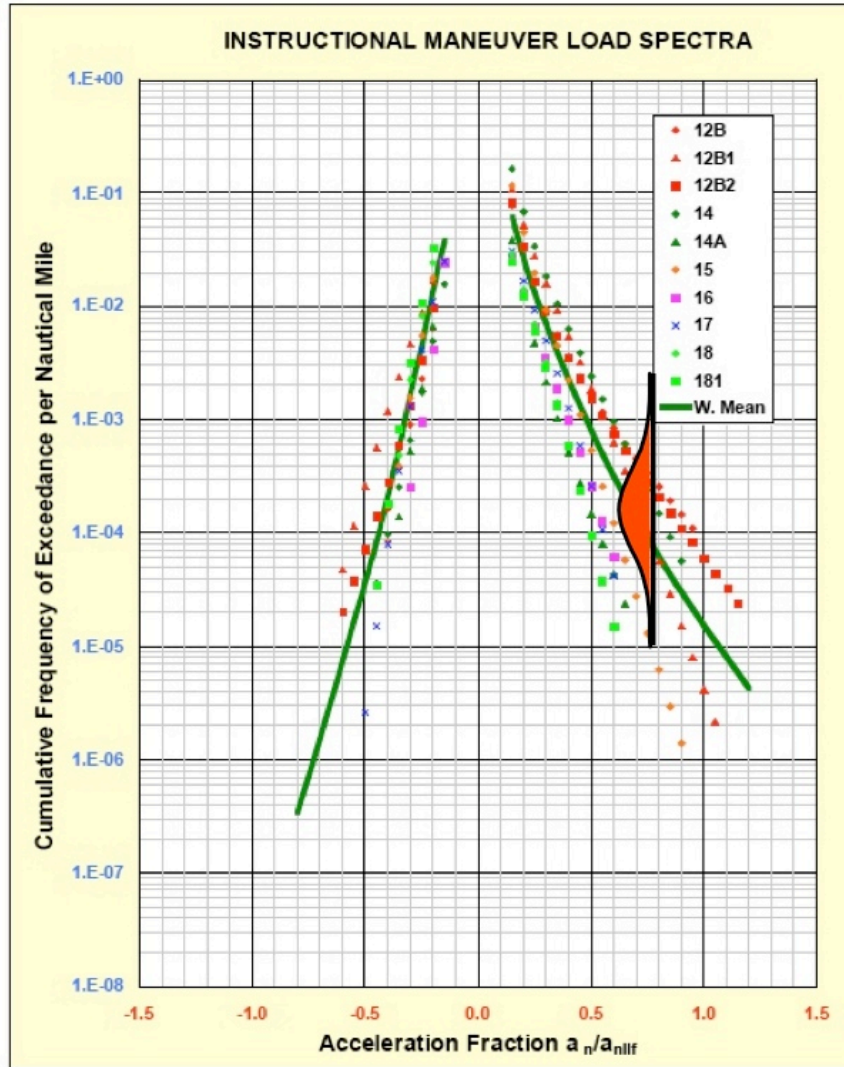


Figure 4. Random maneuver schematic data

The equations used to compute the mean and the COVs in each acceleration fraction level are given below.

$$\log_{10}(\bar{X}) = \frac{1}{n} \sum_{i=1}^n \log(x)_i \quad (1)$$

$$\log_{10}(s) = \frac{\sqrt{\sum_{i=1}^n [\log_{10}(\bar{X}) - \log_{10}(x)_i]^2}}{n-1} \quad (2)$$

$$COV = \frac{\log_{10}(s)}{\log(\bar{X})} \quad (3)$$

where \bar{X} is the estimate of the true mean, μ , of the population based on the new airplane grouping to create statistical data, and s is the estimate of the true standard deviation, σ , of the population based on the new airplane grouping to create statistical data.

Using the equations 1, 2, and 3; the mean and COV for all different usages are calculated as shown in table 4 [5]; the statistical values shown in figure 4 are calculated for each acceleration fraction value.

Table 4. Example calculation of statistical data

Cumulative Freq. per Nautical Mile	Incremental Freq. per Nautical Mile	Log ₁₀ Incremental Freq.
3.5827E-03	1.1843E-03	-2.92654
5.4140E-03	2.2157E-03	-2.65449
3.4972E-03	1.1980E-03	-2.92154
6.3070E-03	2.4377E-03	-2.61302
5.2290E-04	2.4740E-04	-3.60660
2.2364E-03	1.1342E-03	-2.94531
9.9150E-04	4.7620E-04	-3.32221
1.2655E-03	6.7530E-04	-3.17050
5.8090E-04	3.5030E-04	-3.45556
5.9130E-04	3.4930E-04	-3.45680
Mean of Incremental Freq.		1.02684E-03
Mean of Log ₁₀ of Incremental Freq.		-3.10726
Standard Deviation of Log ₁₀ Incremental Freq.		0.34732
COV		0.11178

The methodology for generating random data is showed schematically in figure 5. The process in the code consists of generating a pseudorandom number, then using a polynomial approximation [10] to generate the inverse standard normal. Using the random number, the corresponding mean, and COV, a random variable of gust or maneuver can be generated.

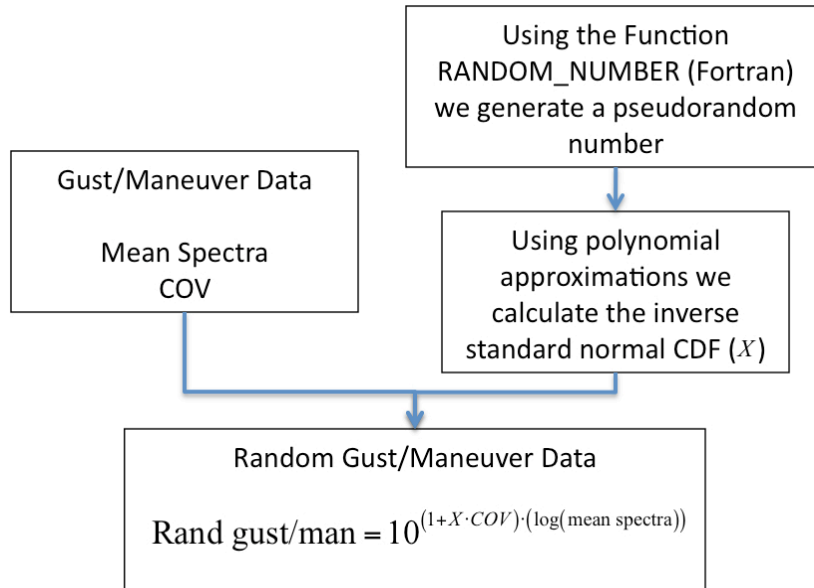


Figure 5. Random gust/maneuver generation flowchart

Frequency data for gust and maneuver often range between two or more orders of magnitude. This makes graphical representations of the data difficult or misleading. To avoid this, it is possible to compress the data by using the logarithm of the frequency data, as shown in table 4. The equation to generate random data (see figure 5) is therefore raised to the power 10.

This process is repeated throughout the exceedance curve by sweeping through the mean values, resulting in a perturbed usage for each Monte Carlo sample. Figure 6 shows the different confident bounds for the data generated for random gust. Figure 7 verifies that the data generated fall within confidence bounds.

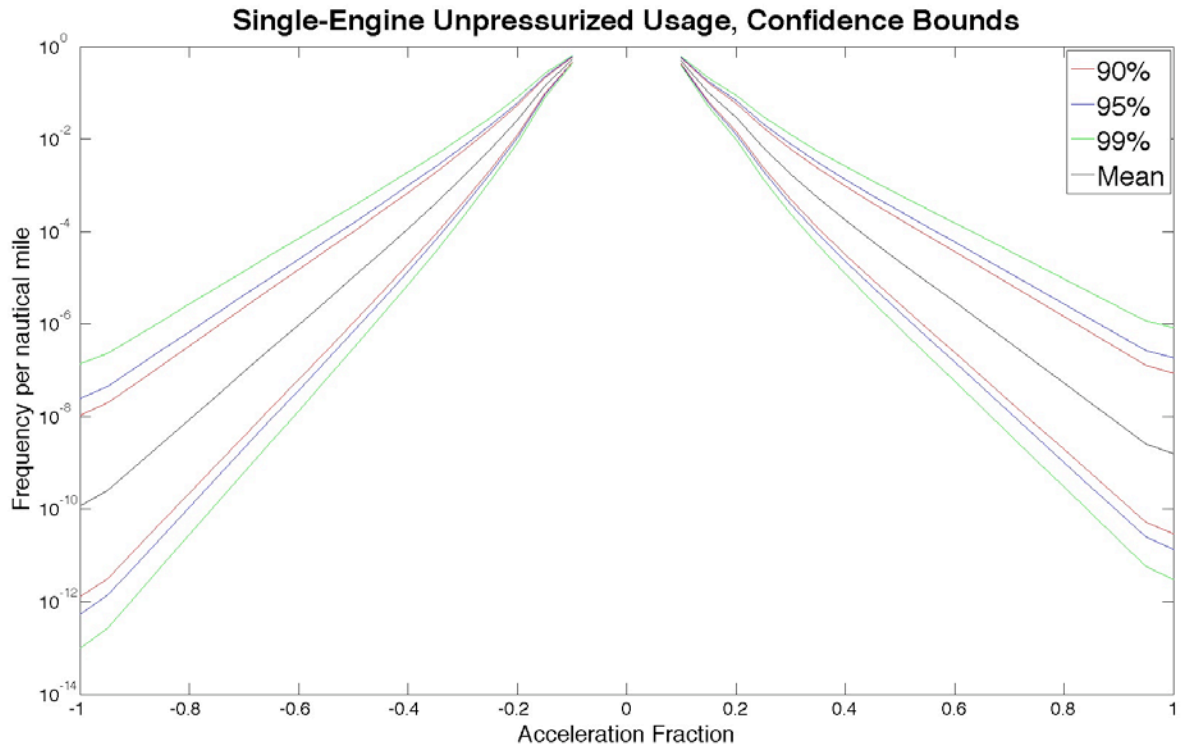


Figure 6. Random gust confidence bounds

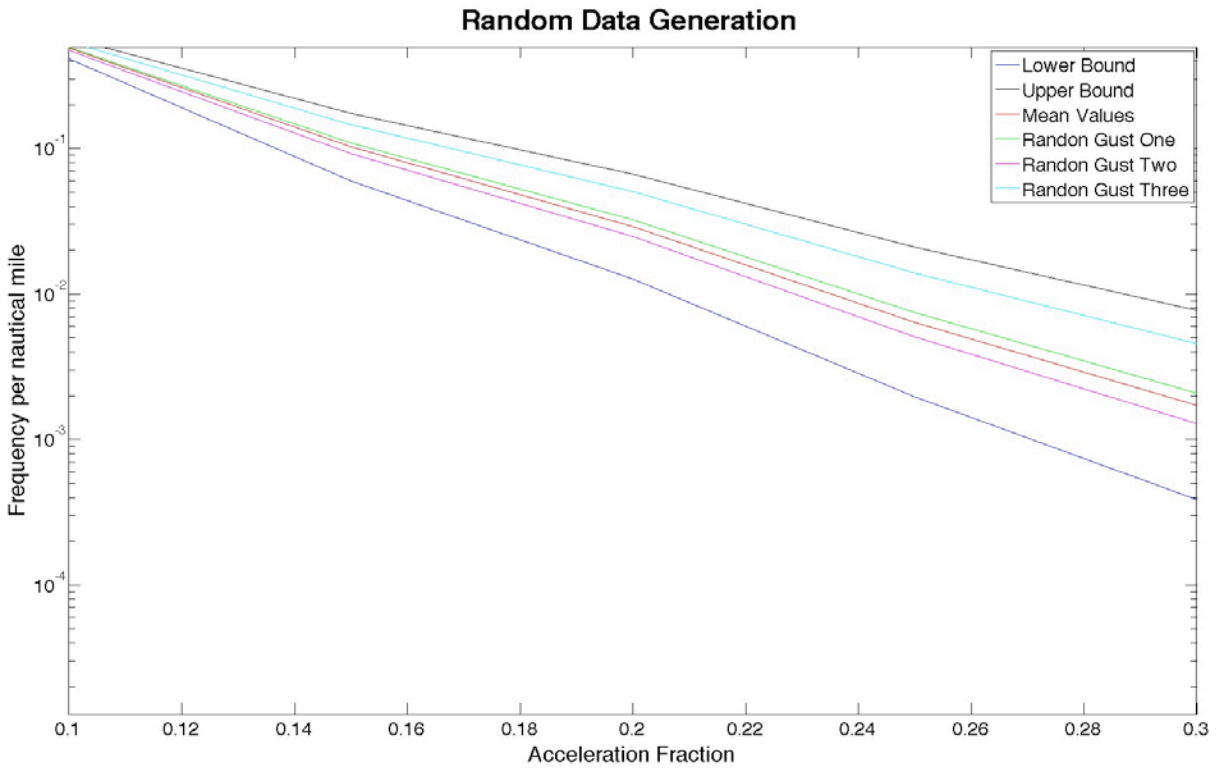


Figure 7. Random gust data generation

2.2.2 Sink Rate

Exceedance information for sink rate velocity can be extracted from FAA report AC23-13A [5] and is presented graphically in figure 8, in which the data are presented as cumulative frequency per 10,000 flights versus sink rate velocity.

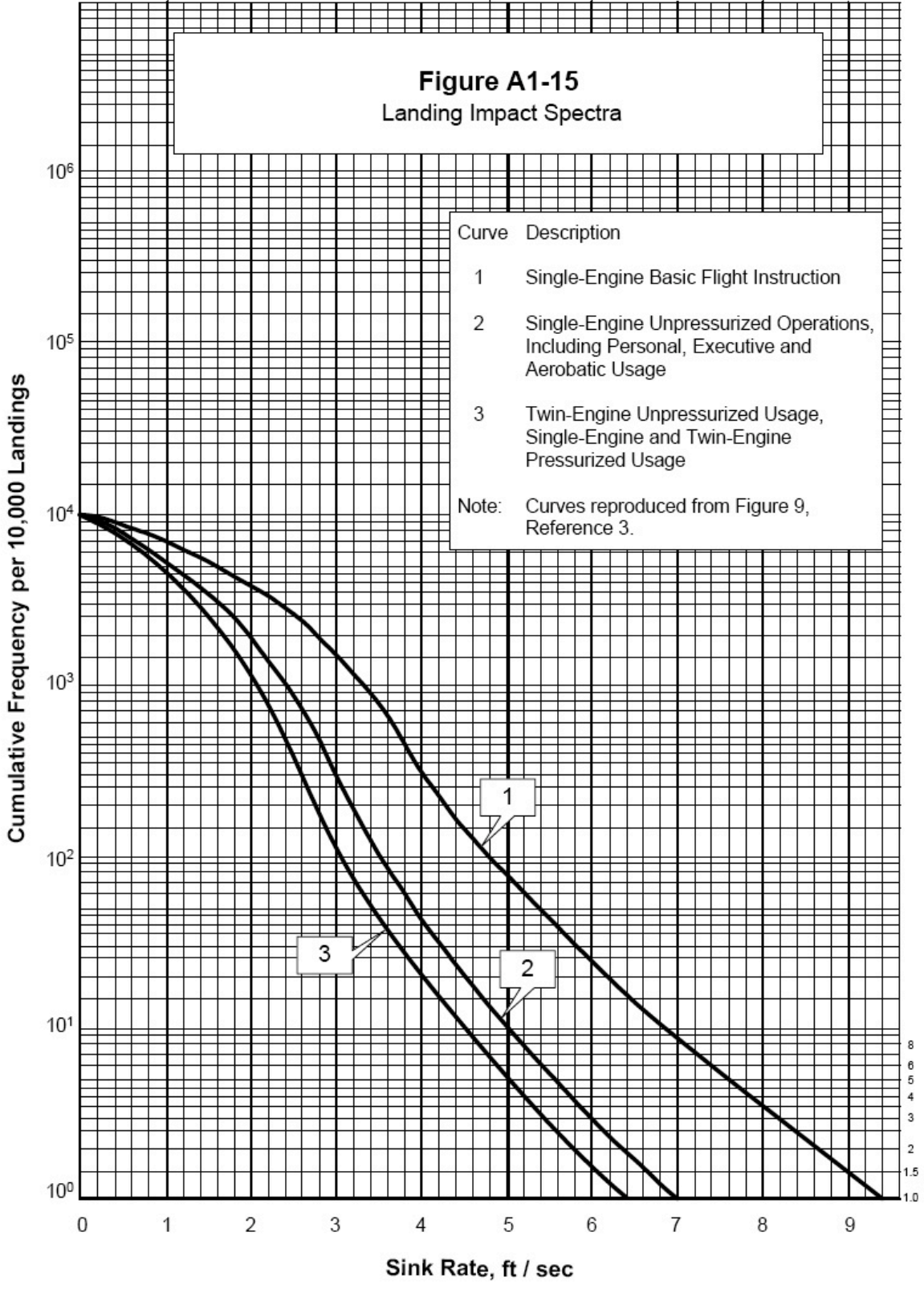


Figure 8. Landing impact spectra

To generate samples from this exceedance curve, it is necessary to convert this information to a cumulative distribution function (CDF). To construct this function, it is necessary to read the information from figure 8. Table 5 is constructed by defining evenly spaced sink rate values and by reading its corresponding cumulative frequency per 10,000 flights. Values in table 5 correspond to single-engine basic flight instruction. If we divide that number by 10,000, we get cumulative frequency per flight (see column 2). Column 3 shows frequency per flight, calculated by subtracting two successive values in column 2. Having this information, the probability distribution function (see column 4 and figure 9) and CDF (see column 5 and figure 10) can be easily created.

To generate realization of this data, a pseudo random number is generated, and then a realization is determined from the CDF.

Table 5. Sink rate CDF construction

Sink Rate Ft/sec	Cumulative Freq. per flight	Freq. per Flight	PDF	CDF
0	1	0	0	0
0.5	0.87	0.13	0.130012351	0.130012351
1	0.69	0.18	0.180017102	0.310029453
1.5	0.52	0.17	0.170016152	0.480045604
2	0.385	0.135	0.135012826	0.615058431
2.5	0.26	0.125	0.125011876	0.740070307
3	0.15	0.11	0.110010451	0.850080758
3.5	0.07	0.08	0.080007601	0.930088358
4	0.03	0.04	0.0400038	0.970092159
4.5	0.014	0.016	0.01600152	0.986093679
5	0.0074	0.0066	0.006600627	0.992694306
5.5	0.0041	0.0033	0.003300314	0.995994619
6	0.0024	0.0017	0.001700162	0.997694781
6.5	0.0014	0.001	0.001000095	0.998694876
7	0.00085	0.00055	0.000550052	0.999244928
7.5	0.00054	0.00031	0.000310029	0.999554958
8	0.00034	0.0002	0.000200019	0.999754977
8.5	0.00022	0.00012	0.000120011	0.999874988
9	0.000145	0.000075	7.50071E-05	0.999949995
9.5	0.000095	0.00005	5.00048E-05	1

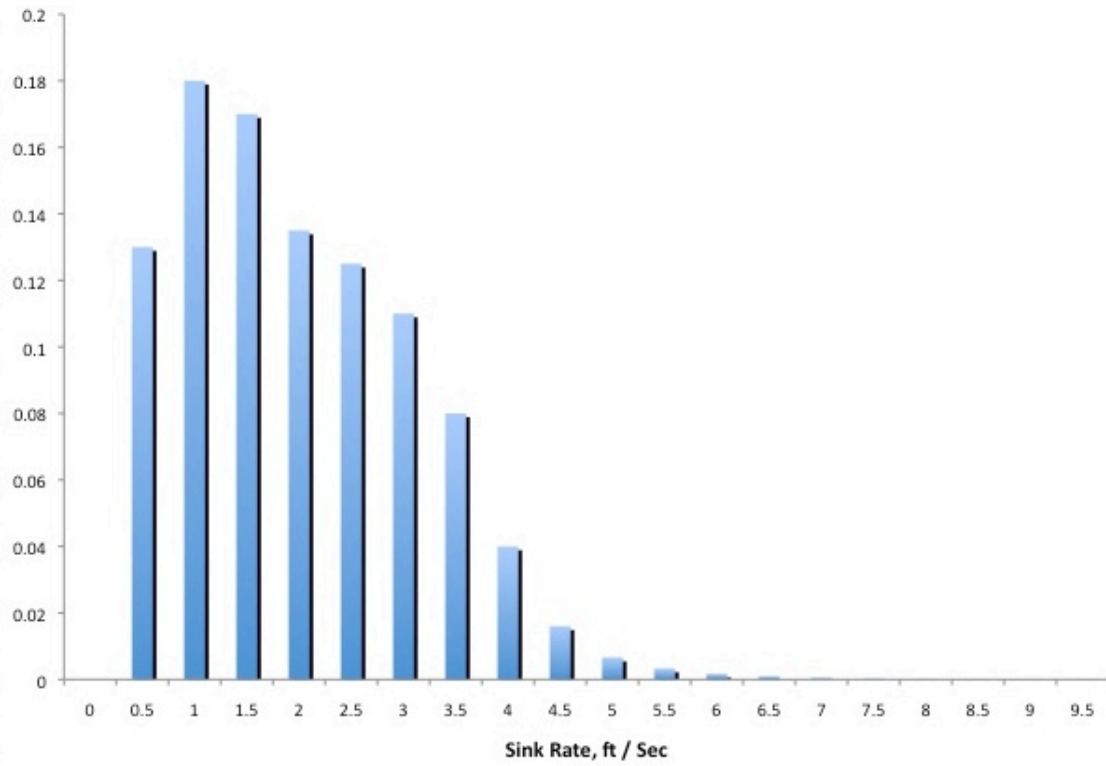


Figure 9. Sink rate probability distribution function

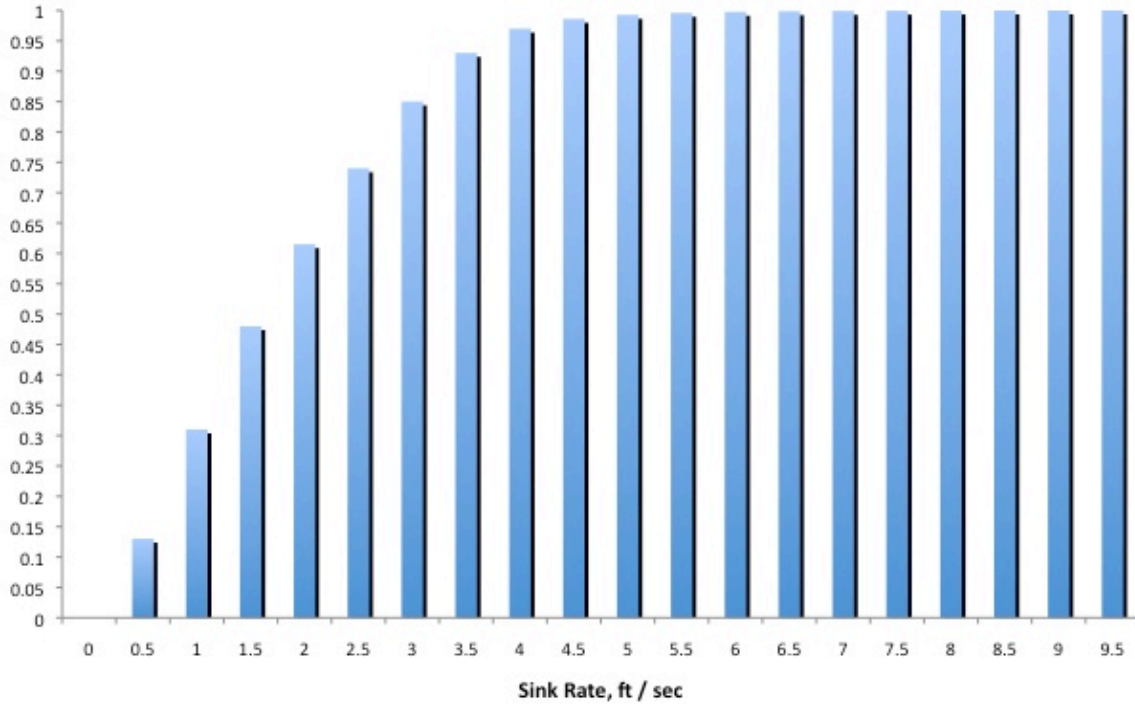


Figure 10. Sink rate CDF

2.2.3 Flight Velocity-Duration

Table 6 shows the kind of statistical data that the user can input for any usage. Up to 13 by 13 data points can be introduced. The data creates a CDF for flight time and for flight speed.

Table 6. Flight length and airspeed data

		Average Speed During Flight, % Design Velocity						
Flight Time (Hours)	% of Flights	1.00	0.95	0.90	0.85	0.80	0.75	0.70
0.25	0	0	0	0	0	0	0	0
0.50	0.05	0	0	0.05	0.25	0.6	0.1	0
0.75	0.15	0	0	0.25	0.4	0.3	0.05	0
1.00	0.35	0.05	0.15	0.45	0.3	0.05	0	0
1.25	0.1	0.05	0.15	0.45	0.3	0.05	0	0
1.50	0.1	0.05	0.3	0.5	0.15	0	0	0
1.75	0.2	0.05	0.3	0.5	0.15	0	0	0
2.00	0.05	0.15	0.55	0.2	0.1	0	0	0

After the code generates the CDFs for flight time and flight speed, a pseudo random number is created, and the flight time is read from its CDF. Because flight velocity and flight time are correlated, the same pseudo random number is used to generate flight velocity. Statistics computed on this data are shown in table 7, and figure 11 shows the created joint probability distribution function from table 6.

Table 7. Flight length and airspeed joint PDF

Flight Time (Hours)	Average Speed During Flight, % Design Velocity						
	1	0.95	0.9	0.85	0.8	0.75	0.7
0.25	0	0	0	0	0	0	0
0.5	0	0	0.0025	0.0125	0.03	0.005	0
0.75	0	0	0.0375	0.06	0.045	0.0075	0
1	0.0175	0.0525	0.1575	0.105	0.0175	0	0
1.25	0.005	0.015	0.045	0.03	0.005	0	0
1.5	0.005	0.03	0.05	0.015	0	0	0
1.75	0.01	0.06	0.1	0.03	0	0	0
2	0.0075	0.0275	0.01	0.005	0	0	0

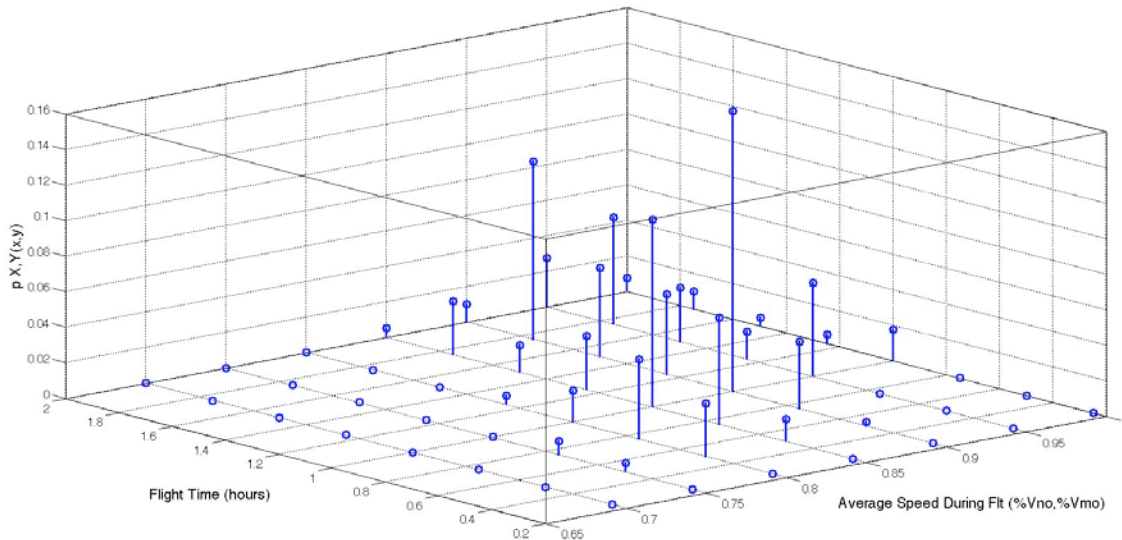


Figure 11. Flight length and airspeed joint PDF

Flight speed values depend on flight time; therefore, values of conditional distribution shown in table 8 are calculated using the following equation:

$$P_{X/Y}(x_i | y_j) \equiv P(X = x_i | Y = y_j) = \frac{P_{XY}(x_i, y_j)}{P_Y(y_j)} \quad (4)$$

where $P_{X/Y}$ is the probability that event X (average speed) occurs given the event Y (flight time).

Table 8. Flight length and airspeed conditionals

Conditionals	Average Speed During Flight (% Vno, % Vmo) → AVS						
	1	0.95	0.9	0.85	0.8	0.75	0.7
p(AVS / 0.25)	0	0	0	0	0	0	0
p(AVS / 0.50)	0	0	0.05	0.25	0.6	0.1	0
p(AVS / 0.75)	0	0	0.25	0.4	0.3	0.05	0
p(AVS / 1.00)	0.05	0.15	0.45	0.3	0.05	0	0
p(AVS / 1.25)	0.05	0.15	0.45	0.3	0.05	0	0
p(AVS / 1.50)	0.05	0.3	0.5	0.15	0	0	0
p(AVS / 1.75)	0.05	0.3	0.5	0.15	0	0	0
p(AVS / 2.00)	0.15	0.55	0.2	0.1	0	0	0

2.2.4 Flight Weight-Duration

The same concept used from the flight duration-velocity matrix is used on the flight weight-duration matrix. Instead of speed percentages, the user inputs weight percentages, which will be used to generate random values for one-g stress and ground stress.

2.2.5 Probabilistic Stress Life

Three different stress-life (S-N) curves have been implemented into the code, one deterministic that is called “AC23” is taken from FAA report AC-23-13A [5]. The other two correspond to P-S-N curves. To construct the P-S-N curves, constant amplitude fatigue test results developed experimentally under a research program by Wichita State University [2, 3] were used. The test data were developed for different coupon configurations at different maximum stress levels and mean stress. A summary of the data available for this study is shown in table 9.

Table 9. Data available to develop P-S-N curves [2,3]

Coupon Configuration	Maximum Stress [KSI]	Number of Data Points	Mean Stress [KSI]
Open hole	42, 32, 18, 12, 10, and 9.25	41	3
Open hole	42, 32, 20, 18, 12.5, and 11.5	46	6
Hi-Lok-filled hole	42, 32, 24, 18, and 14	32	3
Hi-Lok-filled hole	42, 32, 30, 24, 21 and 16	37	6
Rivet-filled hole	46, 42, 32, 30, 21, 17.5, and 14	41	3
Rivet-filled hole	48, 44, 32, 30, 21, 18, and 16	42	6
Hi-Lok 30% load transfer	42, 32, 24, 15, and 8	38	3
Hi-Lok 30% load transfer	42, 32, 24, 15, and 8	38	6
Rivet 6% load transfer	42, 32, 28, 20, and 13	33	3
Rivet 6% load transfer	36, 32, 15, and 13	29	6
Hi-Lok 50% load transfer	42, 32, 24, 15, and 8	37	3
Hi-Lok 50% load transfer	42, 32, 24, 15, and 8	37	6
Rivet 50% load transfer	36, 32, 15, and 13	18	3
Rivet 50% load transfer	42, 32, 28, 20, and 13	23	6

The two probabilistic methods implemented for the S-N curves are explained as follows.

2.2.5.1 American Society for Testing and Materials P-S-N

The ASTM P-S-N curves were constructed by fitting the test data employing “The Standard Practice for Statistical Analysis of Linear or Linearized S-N and Strain-Life (\mathcal{E} -N) Fatigue Data” (ASTM E739) [11]. The method described by the standard assumes that the data are linear in logarithmic space. Run-outs or suspended tests are not included in the fitting. The following equation describes the method:

$$\log N = A + B(\log S) \quad (5)$$

where N is the life at the maximum value of constant amplitude cyclic stress S .

The maximum likelihood estimators of A and B can be calculated using the following equations:

$$\hat{B} = \frac{\sum_{i=1}^k (X_i - \bar{X})(Y_i - \bar{Y})}{\sum_{i=1}^k (X_i - \bar{X})^2} \quad (6)$$

$$\hat{A} = \bar{Y} + \hat{B}\bar{X} \quad (7)$$

where X represents $\log S$, Y represents $\text{Log}N$, and k denotes the number of data points.

Realizations of the ASTM P-S-N curves were randomly generated using an F-distribution and Bernoulli distribution with the following equation (the Bernoulli distribution is used to randomly sample the \pm sign):

$$\hat{Y}_r(X) = \hat{A} + \hat{B}X \pm \sqrt{2F_{v_1, v_2}} \sigma \left[\frac{1}{k} + \frac{(X - \bar{X})^2}{\hat{C}} \right]^{\frac{1}{2}}$$

$$\hat{\sigma}^2 = \frac{\sum_{i=1}^k (Y_i - \hat{Y}_i)^2}{k-2}, \quad \hat{C} = \sum_{i=1}^k (X_i - \bar{X})^2 \quad (8)$$

where F_p denotes the F distribution, k represents the number of data points, and the variance is described by:

$$\hat{\sigma}^2 = \frac{\sum_{i=1}^k (Y_i - \hat{Y}_i)^2}{k-2} \quad (9)$$

Two different ASTM P-S-N curve results are shown in the semi-log space in figures 12–13. Each figure shows the mean value, the 95% confidence bounds (CB), and the test data (blue circles).

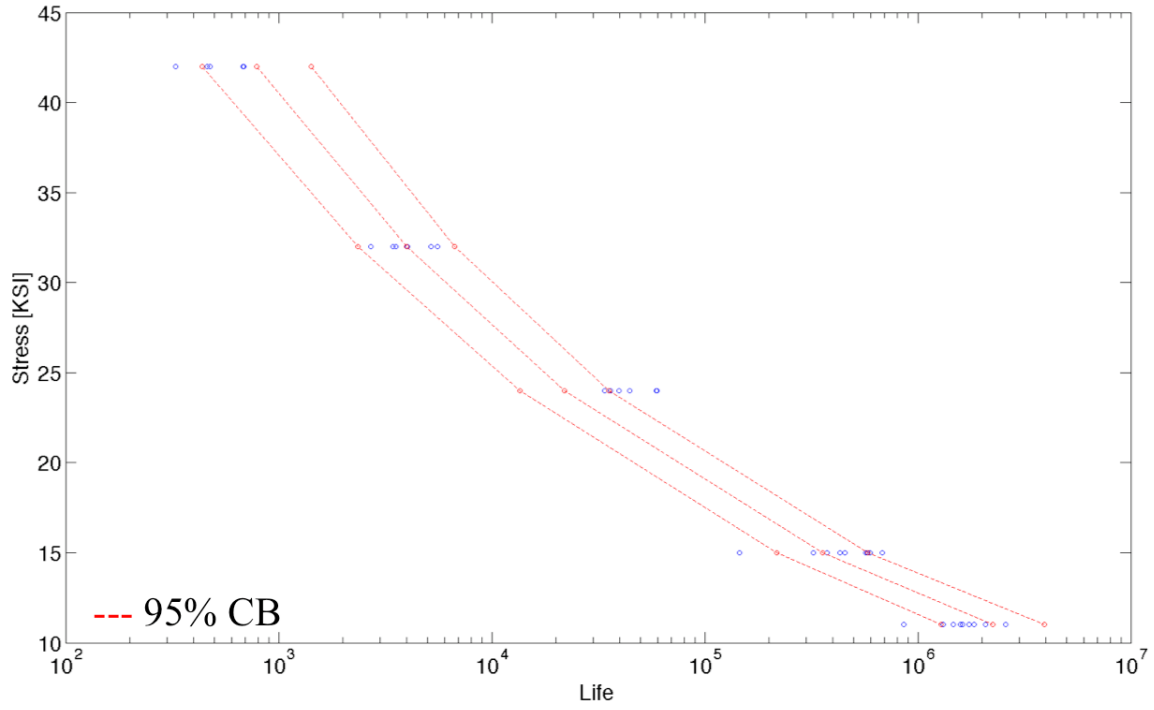


Figure 12. Hi-Lok fastener 6 KSI mean stress 30% load transfer

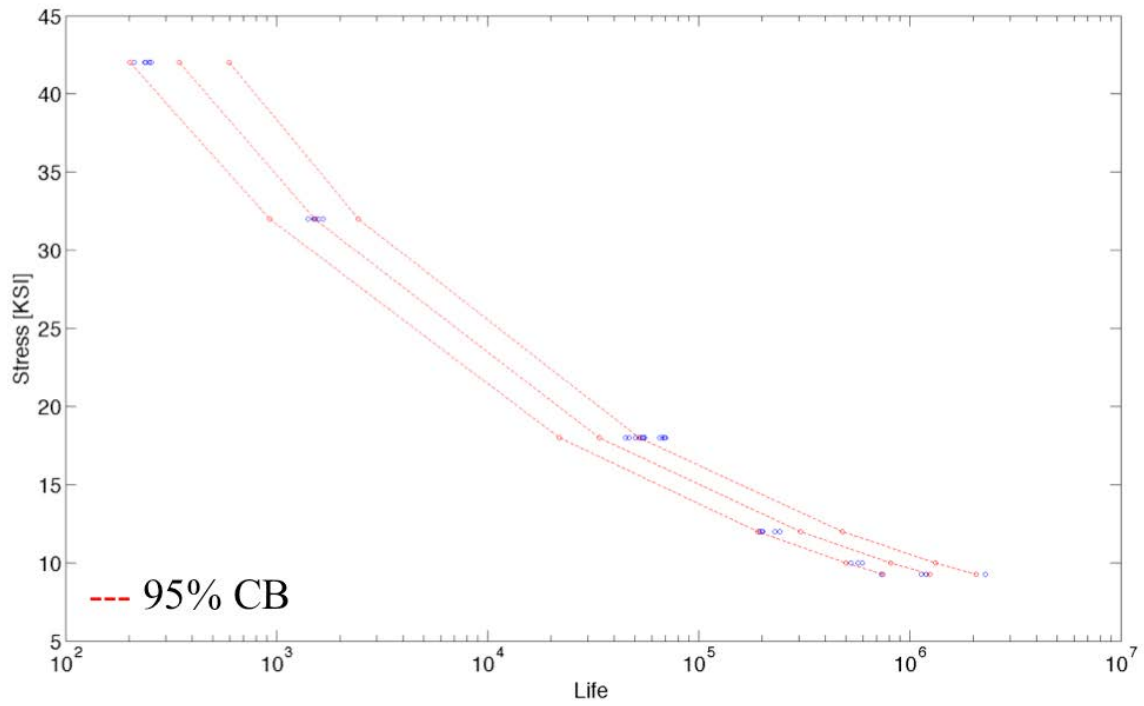


Figure 13. Open hole 3 KSI mean stress

2.2.5.2 Polynomial P-S-N

The polynomial P-S-N curves were constructed by fitting the test data employing up to a fourth-order polynomial equation, excluding all the run outs. The fourth-order polynomial equation is presented as follows:

$$\log(N) = b + C_1(\sigma_{center}) + C_2(\sigma_{center})^2 + C_3(\sigma_{center})^3 + C_4(\sigma_{center})^4 \quad (10)$$

where b represents the intercept from the regression and $\sigma_{center} = \log(S) - \sum_{i=1}^n \frac{\log(S_i)}{n}$.

Realizations of the polynomial P-S-N curves are generated using the residual data with the assumption that the residuals (e) will follow a normal distribution with mean zero and constant standard deviation ($e \sim N(0, \sigma)$). To generate samples using residual information, the following equation is used. D = damage index.

$$\log(N) = b + A(\sigma_{center}) + B(\sigma_{center})^2 + C(\sigma_{center})^3 + D(\sigma_{center})^4 + (Z\sigma_e) \quad (11)$$

where σ_e is the residual standard deviation and $Z \sim N(0,1)$.

If any value in the stress spectrum is smaller than the smallest value in the S-N curve, a linear extrapolation will be made using the two smallest values in the S-N curve.

Three different polynomial P-S-N curve results are shown as follows: figures 14–16 show the mean predicted value in blue, the 95% CB in red, and the test data (black circles).

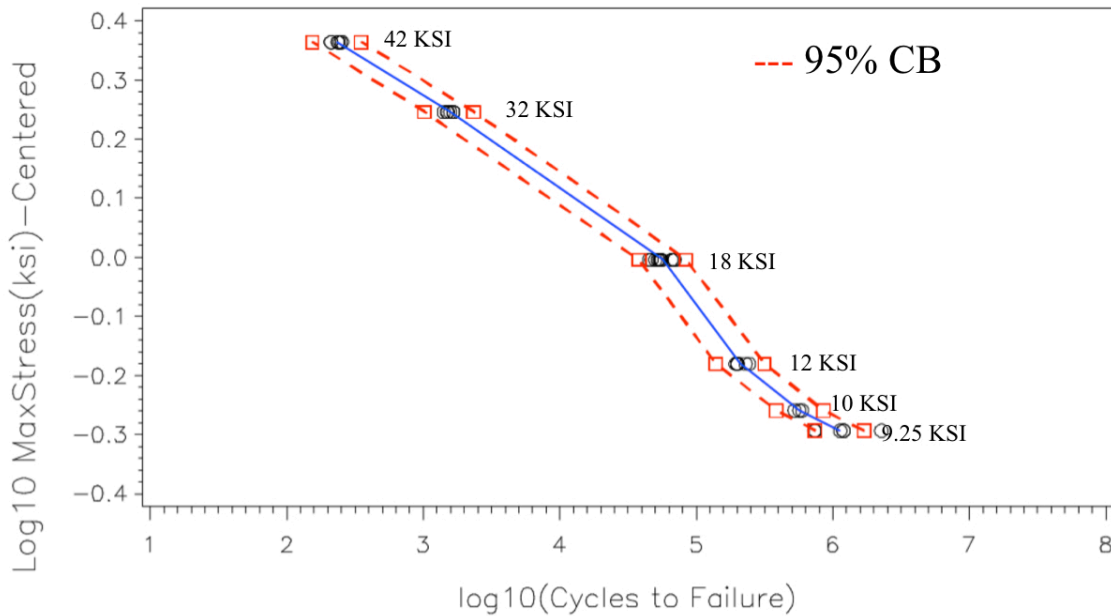


Figure 14. Open hole 3 KSI mean stress

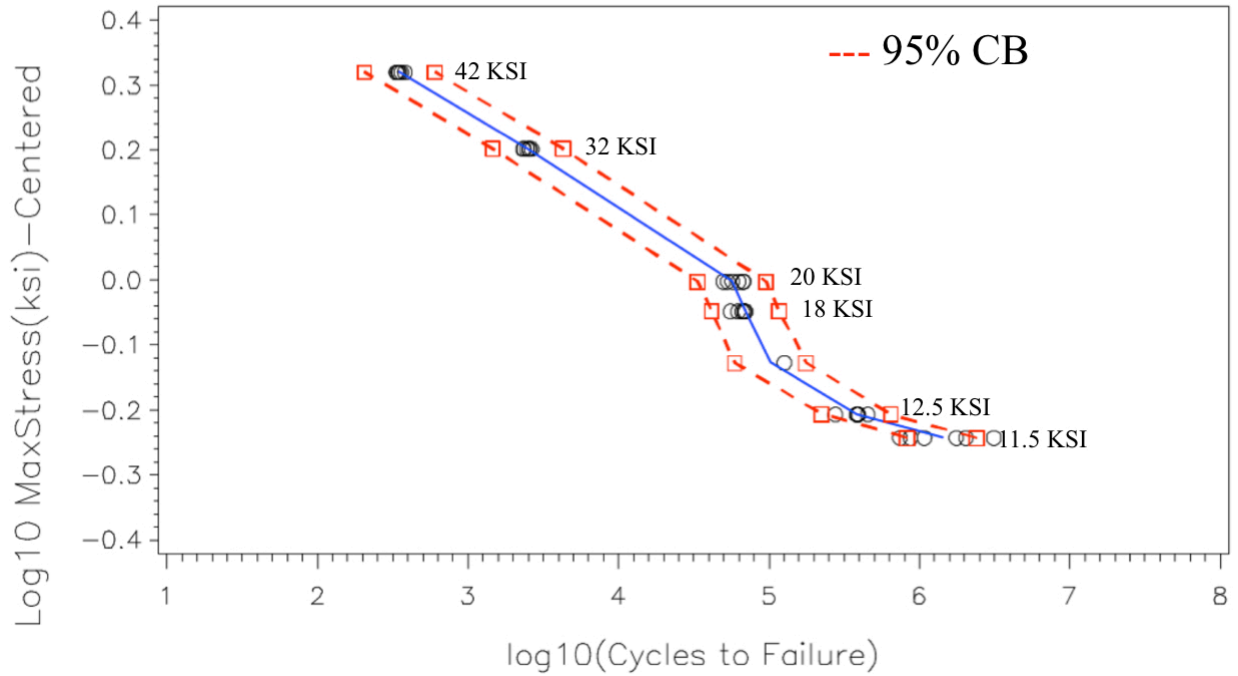


Figure 15. Open hole 6 KSI mean stress

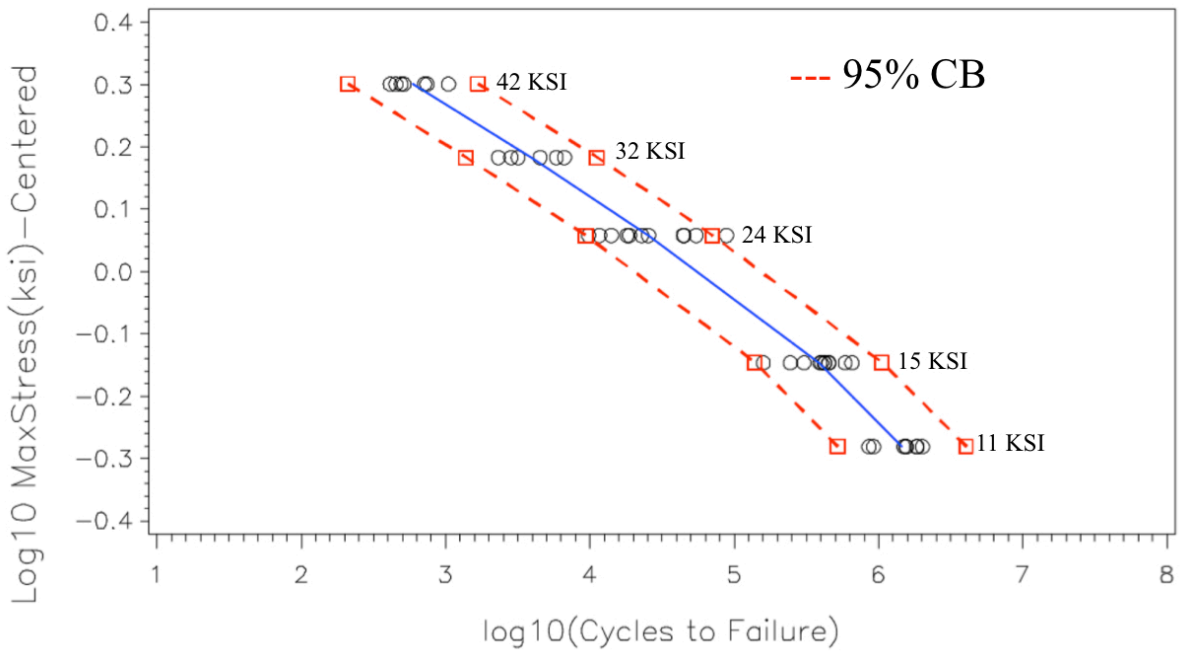


Figure 16. Hi-Lok fastener 6 KSI mean stress 50% load transfer

2.2.6 Stress Severity Factor

The stress severity factor (SSF) [12] is a fatigue quality number that emphasizes the fatigue characteristics of the structure rather than its static strength.

The SSF is defined by the following equation:

$$SSF = \frac{\alpha \cdot \beta}{S} \left(K_{tb} \times \theta \times \frac{\Delta P}{d \cdot t} + K_{tg} \times \frac{P}{w \cdot t} \right) \quad (12)$$

where K_{tg} is the stress concentration factor for the gross area, K_{tb} is the stress concentration factor for the bearing stress, P is the bypassing load, ΔP is the load transfer through the fastener, α accounts for the hole quality, β is the hole-filling factor that accounts for the interference between the fastener and the hole, θ is the bearing distribution factor that accounts for the effect of non-uniformity of bearing stress on the hole surface, w is the width of the specimen, t is the thickness of the specimen, and d is the diameter of the fastener (see figure 17).

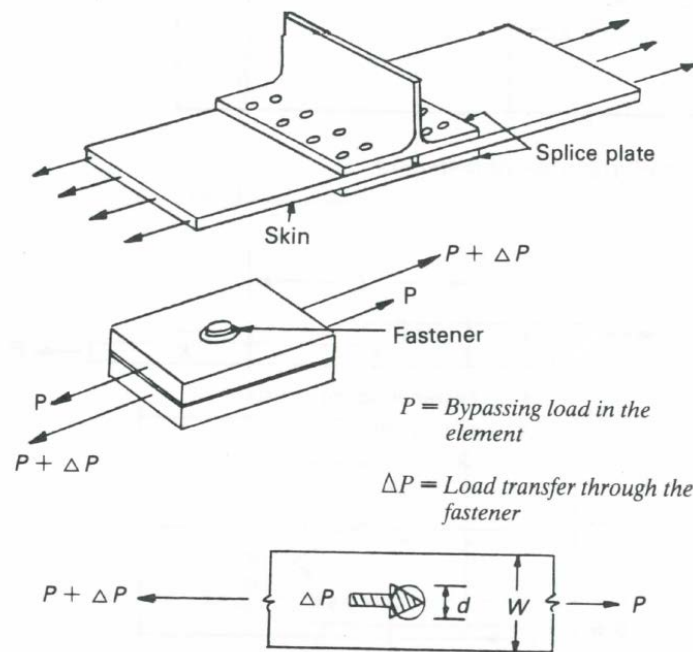


Figure 17. Load fastener, load transfer, and bypass load

The different parameters of the SSF can be developed for different specimens for which the amount of transferred load and bypass load is known. The hole quality value α is 1.0 for standard holes and 0.9 for drilled and reamed holes. The SSF can be written as a function of the unknown parameters, β and θ , by identifying the ratios of fatigue strength of different specimens with the inverse ratios of their SSF numbers [12].

The β parameter is developed using the tested open hole (OH) data and the tested filled hole (FH) data. To generate the parameter, it is necessary to identify the ratios of fatigue strength with the inverse ratios of their SSF numbers, as shown in equation 13 and in figure 18.

$$\frac{S(N_f)_{OH}}{S(N_f)_{FH}} = \frac{SSF_{FH}}{SSF_{OH}} \quad (13)$$

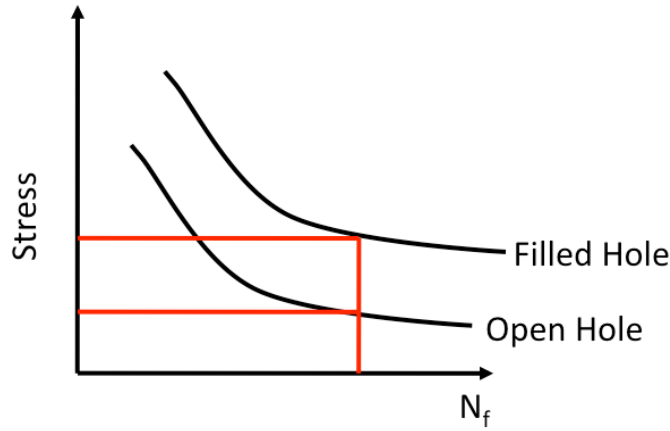


Figure 18. Hi-Lok 30% load transfer 3 KSI mean stress

To generate β as a function of life, it is necessary to sweep through the life values and read the stress values $S(N_f)$ for the OH and FH configurations at that specific life. Then, assuming by definition $\beta_{OH} = 1$, $\alpha_{OH} = 1$, $\alpha_{FH} = 1$ and knowing that for FH and OH the load transfer is zero, β_{FH} can be computed from equation 15. K_{tg} values cancel out because the geometry of both coupons is the same.

$$\frac{S(N_f)_{OH}}{S(N_f)_{FH}} = \frac{\alpha_{FH} \cdot \beta_{FH} \cdot K_{tg}}{\alpha_{OH} \cdot \beta_{OH} \cdot K_{tg}} \quad (14)$$

The results indicate that:

$$\beta_{FH}(N_f) = \frac{\alpha_{OH} \cdot \beta_{OH} \cdot S(N_f)_{OH}}{\alpha_{FH} \cdot S(N_f)_{FH}} \quad (15)$$

where S denotes the far field stress.

Having the values for β , the values for the θ for the different load transfer configurations can be computed using equation 17. β_{FH} in this equation can be read from the β figures in the results section according to the maximum and mean stress. α_{OH} and α_{FH} are assumed equal. The stress concentration factor for the gross area (K_{tg}) and the stress concentration factor for the bearing stress (K_{tb}) can be found in reference Niu, C.Y., "Airframe Structural Design." [13].

$$\frac{S(N_f)_{OH}}{S(N_f)_{FH}} = \frac{\alpha_{FH} \cdot \beta_{FH} \left\{ K_{tb} \cdot \theta \cdot LT \cdot \frac{w}{d} + K_{tb}(1-LT) \right\}}{\alpha_{OH} \cdot \beta_{OH} \cdot K_{tg}} \quad (16)$$

Values of θ for the Hi-Lok configuration are shown in the results section. Rearranging, the equation for θ yields:

$$\theta = \frac{\frac{S(N_f)_{OH} \cdot \beta_{OH} \cdot K_{tg}}{S(N_f)_{FH} \cdot \beta_{FH}} - K_{tb}(1-LT)}{K_{tg} \cdot LT \cdot w/d} \quad (17)$$

Finally, having β and θ , the SSF as a function of the far field stress can be calculated using the following equation:

$$SSF = \alpha\beta \left(K_{tb} \times \theta \times LT \times \frac{w}{d} + K_{tg}(1-LT) \right) \quad (18)$$

where $LT = \Delta P / P$

Using the assumption presented in equation 13, the SSF can be used to predict different S-N curves. For example, given the S-N data for OH (SSF = 3), the life for SSF = 2.6 can be calculated as follows. Equation 7 can be rewritten as:

$$\frac{S_{\max}(N_f)^{\text{@ SSF}_{Any}}}{S_{\max}(N_f)^{\text{@ SSF}_{OH}}} = \frac{SSF_{OH}}{SSF_{Any}} \quad (19)$$

and the SSF ratio calculated as:

$$SSF \text{ Ratio} = \frac{SSF_{OH}}{SSF_{Any}} = \frac{3}{2.6} = 1.15 \quad (20)$$

With this SSF ratio, the S-N curve for SSF = 2.6 can be calculated as shown in equation 21 and figure 19:

$$S_{\max}^{\text{@ SSF}_{Any}} = (SSF \text{ Ratio}) \cdot S_{\max}^{\text{@ SSF}_{OH}} \quad (21)$$

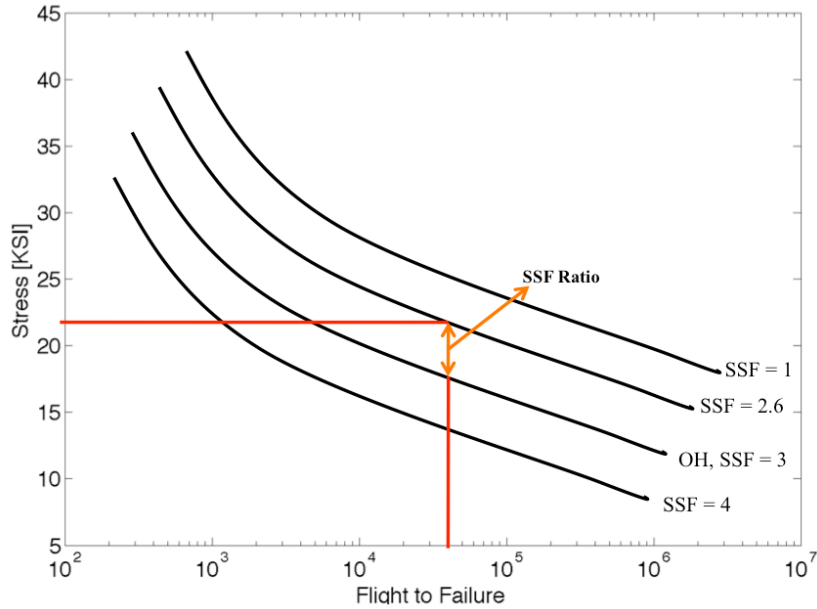


Figure 19. S-N prediction using OH data and SSF

2.2.7 Miner's damage index

Miner's rule dictates that failure occurs when the damage index (D) exceeds 1. However, numerous comparisons with test results show that failure occurs for a range of damage index values, and the results are case and material dependent. For this reason, probability distributions of damage index were developed as a function of SSFs and spectrum types through simulations of variable amplitude tests [2,3].

The methodology to generate the failure damage index is briefly explained as follows:

- As shown in figure 20, stress spectrums for three different aircraft usages (special, normal, and acrobatic) and three stress levels (low, medium, and high) were generated using the guidelines contained in FAA report AFS-120 [4]. The stress spectrum was used for the variable amplitude testing to compute the flights/cycles-to-failure.

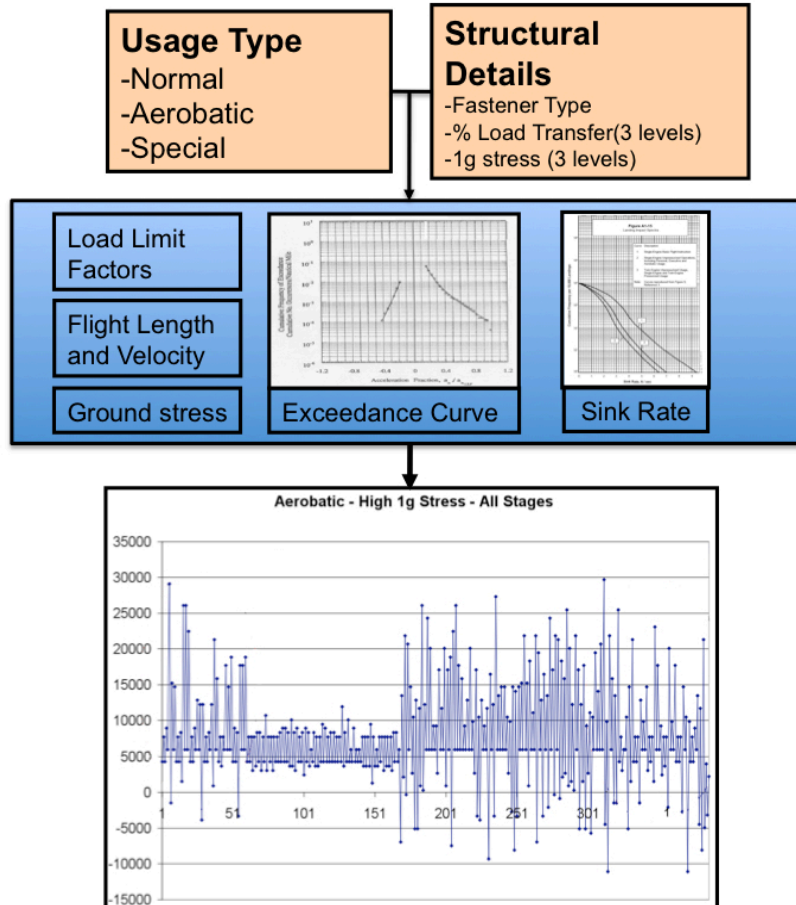


Figure 20. Random miner's stress spectrum flowchart

- Utilizing the same spectrums used during testing and the P-S-N curves developed from constant amplitude tests, the life for each stress pair within the spectrum was calculated and stored. The spectrum was repeated until the number of simulated flights equaled the flights-to-failure from test. At the end, the damages for each of the load pairs for all the flights simulated from the spectrum results were added and the failure index determined (see figure 21).
- The process was repeated for the total number of variable amplitude tests, 10 for normal and 6 for acrobatic; and then replicated inside a Monte Carlo simulation for different realizations of S-N curves. Using this data, failure damage index probability distributions were developed.

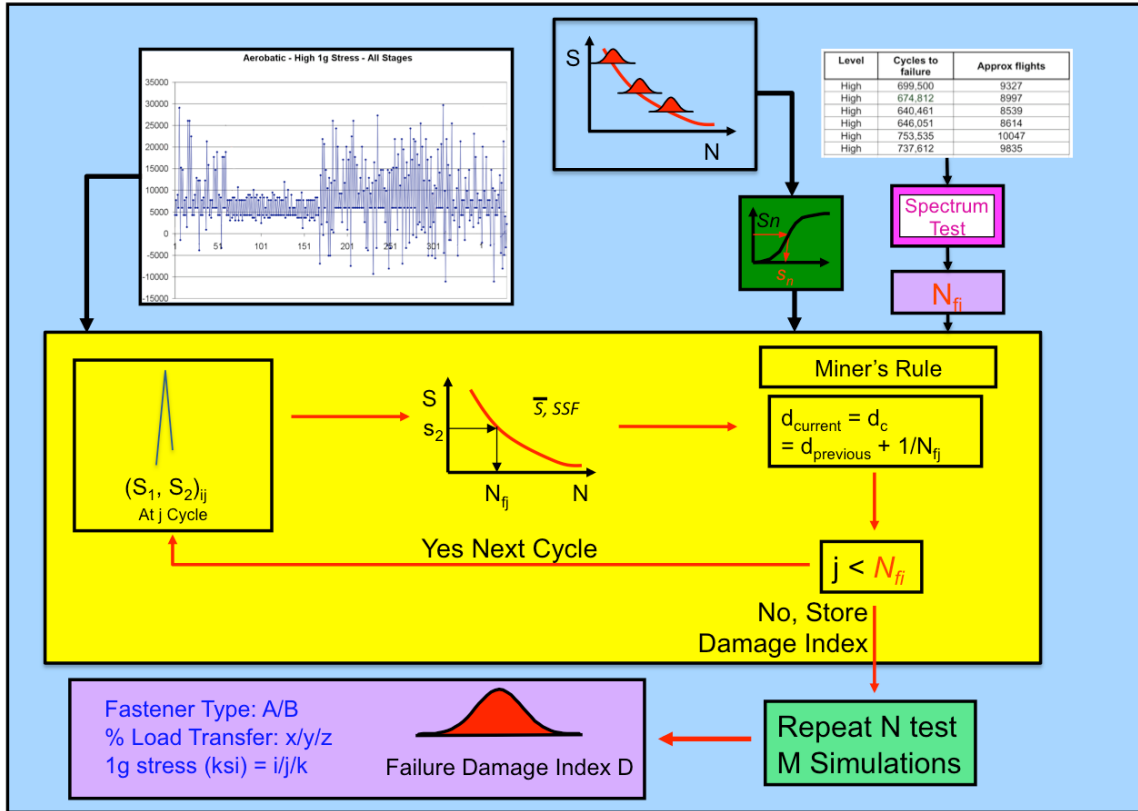


Figure 21. Random Miner's damage index accumulation flowchart

The damage index values results were tested against a number of probability distributions to determine the best fit. The Weibull distribution was the best distribution for all the different cases, according to Kolmogorov-Smirnov, Anderson-Darling, and Chi-Squared tests, for goodness of fit and from probability plots.

Some of the random failure damage index values are summarized in table 10.

Table 10. Random damage index summary results

P-S-N Curve	Spectrum	Severity	Coupon Configuration	Mean Damage Index	COV
ASTM	Normal	High (9 KSI)	Open hole	0.7248	0.113
ASTM	Normal	Medium (7 KSI)	Open hole	0.8774	0.190
ASTM	Normal	Low (5 KSI)	Open hole	0.7281	0.228
ASTM	Normal	High (9 KSI)	50% load transfer	5.7379	0.483
ASTM	Normal	Medium (7 KSI)	50% load transfer	2.2056	0.437
Poly	Normal	High (6 KSI)	Open hole	1.4095	0.0686
Poly	Normal	Med. (4.5 KSI)	Open hole	0.4239	0.1329
Poly	Normal	High (6 KSI)	50% load transfer	5.5526	0.3674
Poly	Normal	Med. (4.5 KSI)	50% load transfer	3.4582	0.1790

The following figures 22–24 present the PDFs for some of the results.

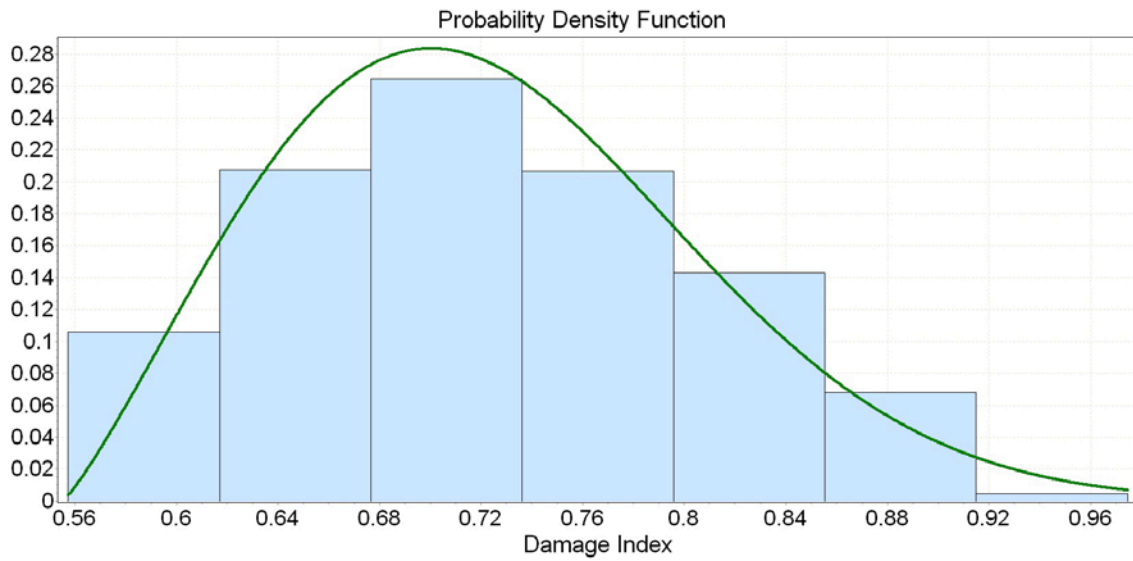


Figure 22. PDF normal usage, high severity, and OH

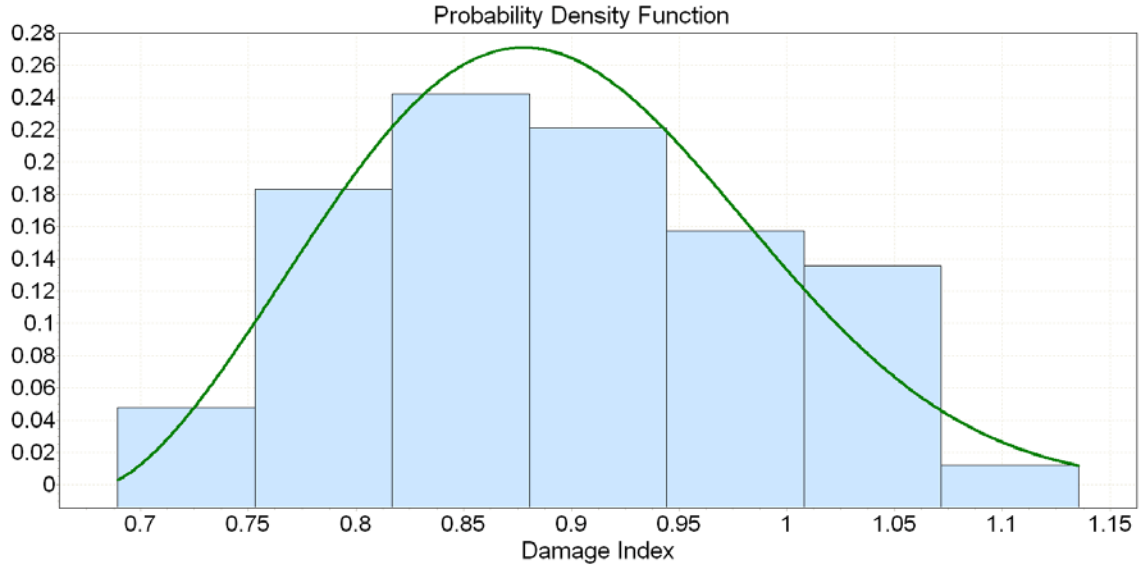


Figure 23. PDF aerobic usage, high severity, and OH

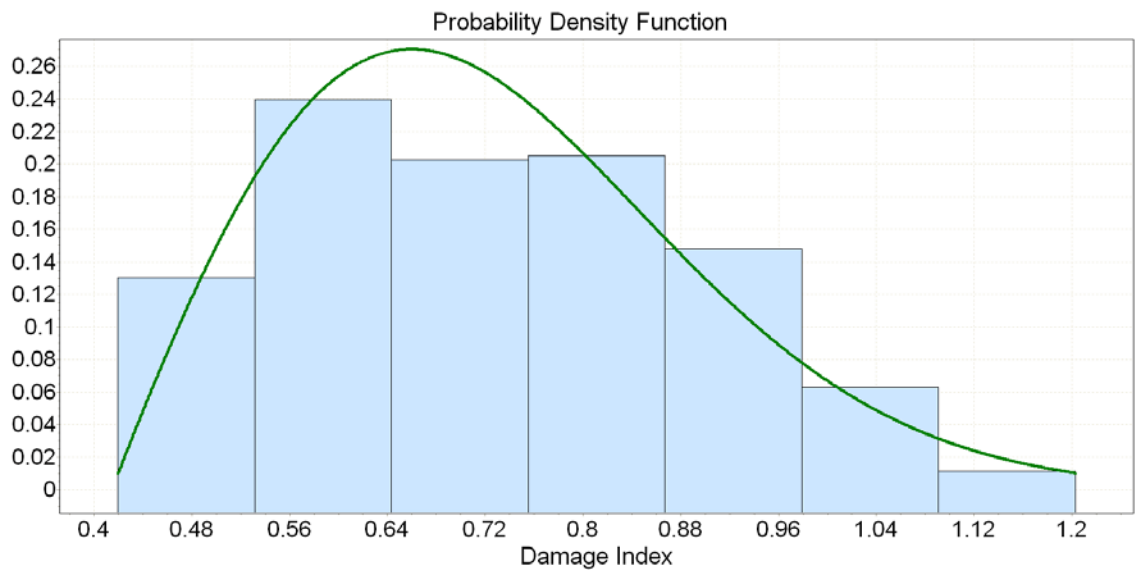


Figure 24. PDF normal usage, low severity, and OH

The code allows the user to input the parameters for normal distribution (mean and the standard deviation) or the parameters for Weibull distribution (scale, shape, and location). If normal distribution is selected, the mean and the standard deviation are needed. The code then uses a pseudo random number from a standard normal distribution to calculate the random damage index value using the following equation:

$$Random_D = (pseudo_number) \cdot (Damage_std_dev) + Damage_mean \quad (22)$$

If Weibull distribution is selected, the scale, shape, and location parameters are needed. The code uses a pseudo random number from a standard normal distribution to calculate the random damage index value using the following equation:

$$Random_D = scale \cdot \log\left(\frac{1}{1 - pseudo_number}\right)^{\frac{1}{shape}} + location \quad (23)$$

2.3 NUMERICAL EXAMPLES

Two numerical examples are presented to demonstrate the methodology. For the first example, the airplane was assumed to have flown in a mixed usage, first instructional usage, and then personal usage in equal periods of time: 50% in instructional usage and 50% in personal usage using the damage mode with probabilistic S-N curve and probabilistic loading. For the second example, the airplane was assumed to have flown for 10,800 hours on instructional usage and was flown for 2,000 hours on personal usage, thereafter using the hours mode with deterministic S-N curve (AC23-13A) [5] and deterministic loading.

Probability distributions for the inputs have been investigated and developed for both usages. Table 11 and figure 25 show correlated flight length and flight velocity data for instructional usage.

Table 11. Flight length and airspeed data for instructional usage

		Average Speed During Flight, % Design Velocity						
Flight Time (Hours)	% of Flights	1.00	0.95	0.90	0.85	0.80	0.75	0.70
0.25	0	0	0	0	0	0	0	0
0.50	0.05	0	0	0.05	0.25	0.6	0.1	0
0.75	0.15	0	0	0.25	0.4	0.3	0.05	0
1.00	0.35	0.05	0.15	0.45	0.3	0.05	0	0
1.25	0.1	0.05	0.15	0.45	0.3	0.05	0	0
1.50	0.1	0.05	0.3	0.5	0.15	0	0	0
1.75	0.2	0.05	0.3	0.5	0.15	0	0	0
2.00	0.05	0.15	0.55	0.2	0.1	0	0	0

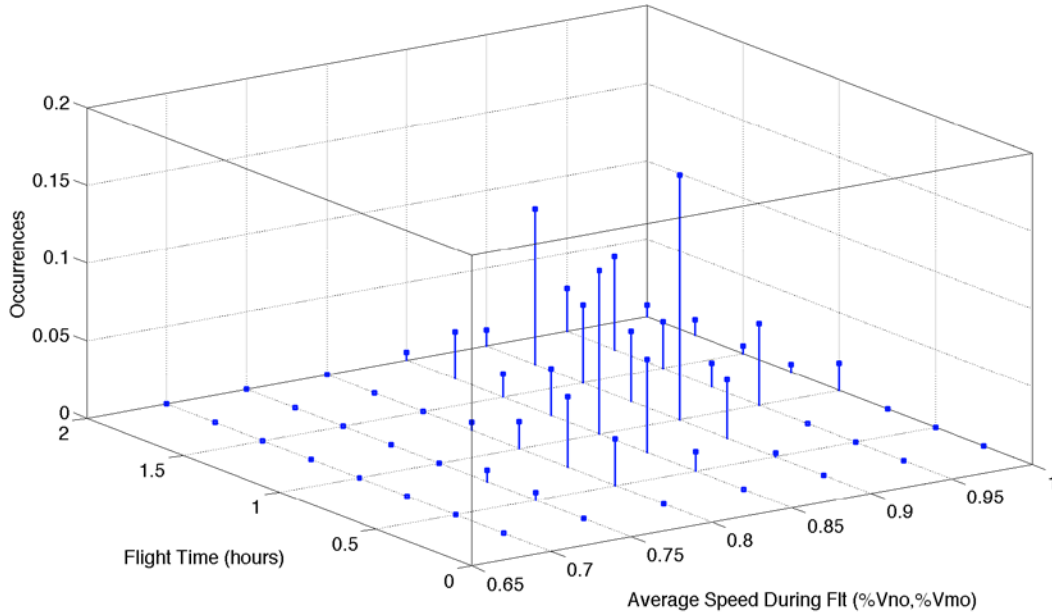


Figure 25. Flight length and flight velocity joint PDF for instructional usage

Table 12 and figure 26 show flight length and flight velocity data for personal usage. Exceedance curves and sink rate data were developed from the AC 23-13A [5]. Flight length and weight data for instructional and personal usage are also provided in table 13.

Table 12. Flight length and airspeed data for personal usage

		Average Speed During Flight, % Design Velocity					
Flight Time (Hours)	% of Flights	1.00	0.95	0.90	0.85	0.80	0.75
1.00	0.35	0.05	0.15	0.45	0.3	0.05	0
1.25	0.1	0.05	0.15	0.45	0.3	0.05	0
1.50	0.1	0.05	0.3	0.5	0.15	0	0
1.75	0.2	0.05	0.3	0.5	0.15	0	0
2.00	0.25	0.15	0.55	0.2	0.1	0	0

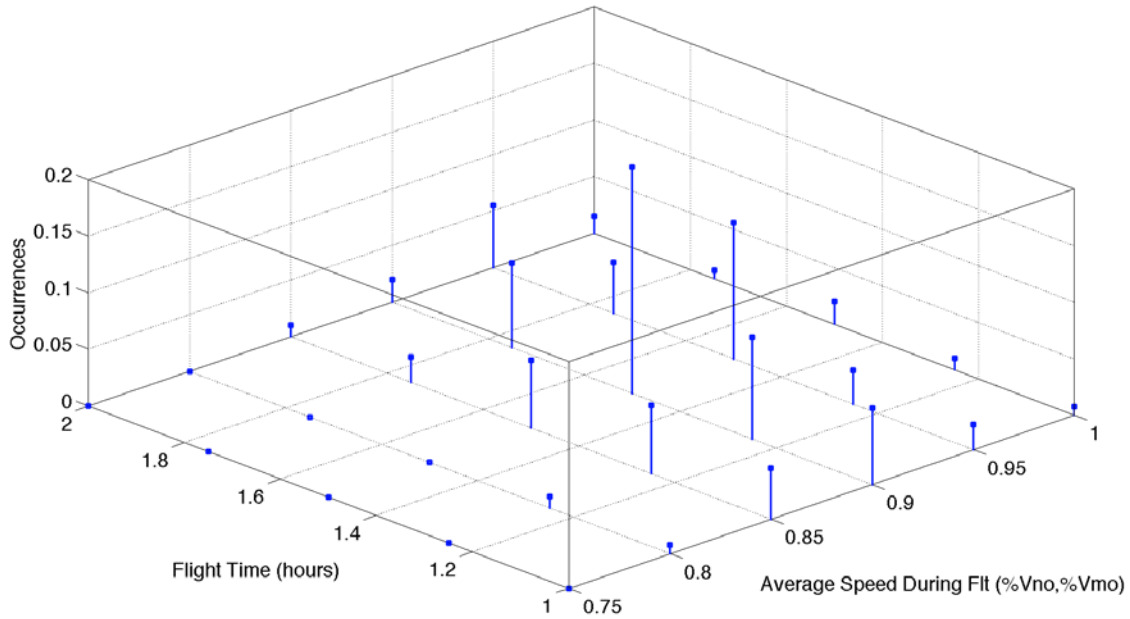


Figure 26. Flight length and flight velocity joint PDF for personal usage

Table 13. Flight length and weight data for instructional and personal usage

		Weight Percentage		
Flight Time (Hours)	% of Flights	1.00	0.95	0.90
1.00	0.4	0.10	0.00	0.90
1.50	0.0	0.00	0.00	0.00
2.00	0.6	0.10	0.00	0.90

2.3.1 Damage Mode

A safe-life and sensitivity analysis was conducted to determine the flights/hours-to-failure, taking into account both usages. The data used for this analysis is contained in table 14.

Table 14. Analysis data

Variable	Characteristics	
Gust/maneuver load exceedances	Probabilistic exceedances curves for instructional and personal usage were taken from reference 1.	
Sink rate	Sink rate values were taken from reference 5.	
Maneuver load limit factors	Instructional usage	+2.80 -2.50
	Personal usage	+2.40 -2.20
Gust load limit factors	Instructional usage	+2.15 -2.15
	Personal usage	+2.30 -2.30
One-g stress	Instructional usage	+7410
	Personal usage	+7900
Ground stress	Instructional usage	-4520
	Personal usage	-4800
Aircraft velocity	Instructional usage	160
	Personal usage	170
Damage index	Normal distribution with mean 1.0 and standard deviation 0.2	

This analysis was performed using a weighted usage analysis (i.e., it was assumed that the airplane was used 50% of the time in instructional usage and 50% of the time in personal usage). There were 20,000 samples run, and table 15 shows the statistical results obtained from the analysis.

Table 15. Safe-life analysis results

Confidence Bounds			Hours-to-Failure Results	Confidence Bounds		
99%	95%	90%	Mean	90%	95%	99%
40,923.4	41,032.1	41,089.1	41,381.3	41,673.6	41,730.6	41,839.3
99%	95%	90%	Standard Deviation	90%	95%	99%
24,880.1	24,956.3	24,995.4	25,200.8	25,409.9	25,450.2	25,529.3
Confidence Bounds			Flights-to-Failure Results	Confidence Bounds		
99%	95%	90%	Mean	90%	95%	99%
33,646	33,766	33,829	34,152	34,474	34,537	34,657
99%	95%	90%	Standard Deviation	90%	95%	99%
27,479	27,563	27,607	27,834	28,065	28,109	28,196

Probability plotting versus different PDFs is shown in figure 27. The flights-to-failure distribution clearly follows a lognormal distribution. The PDFs of flights-to-failure and hours-to-failure are shown in figures 28 and 29, respectively.

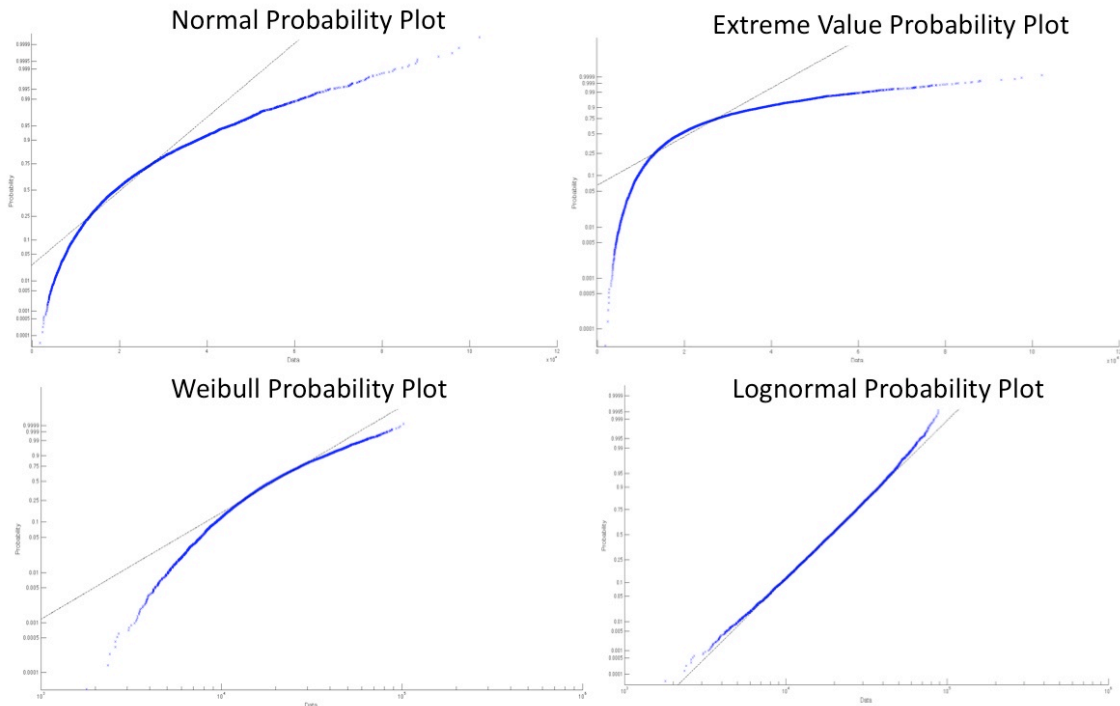


Figure 27. Flights-to-failure probability plot testing

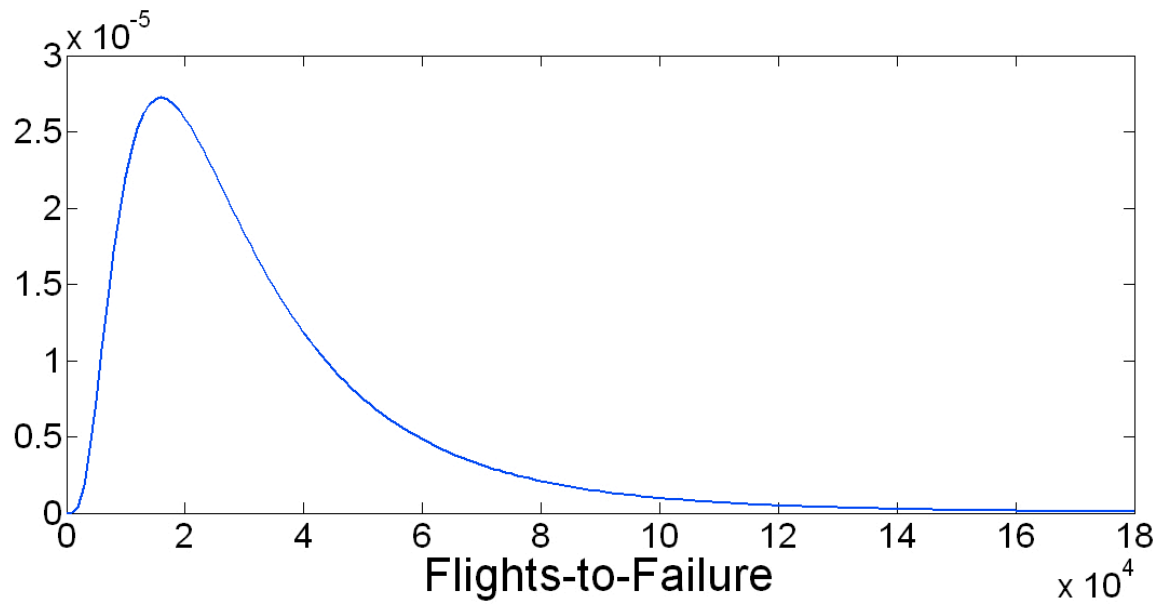


Figure 28. Flights-to-failure PDF

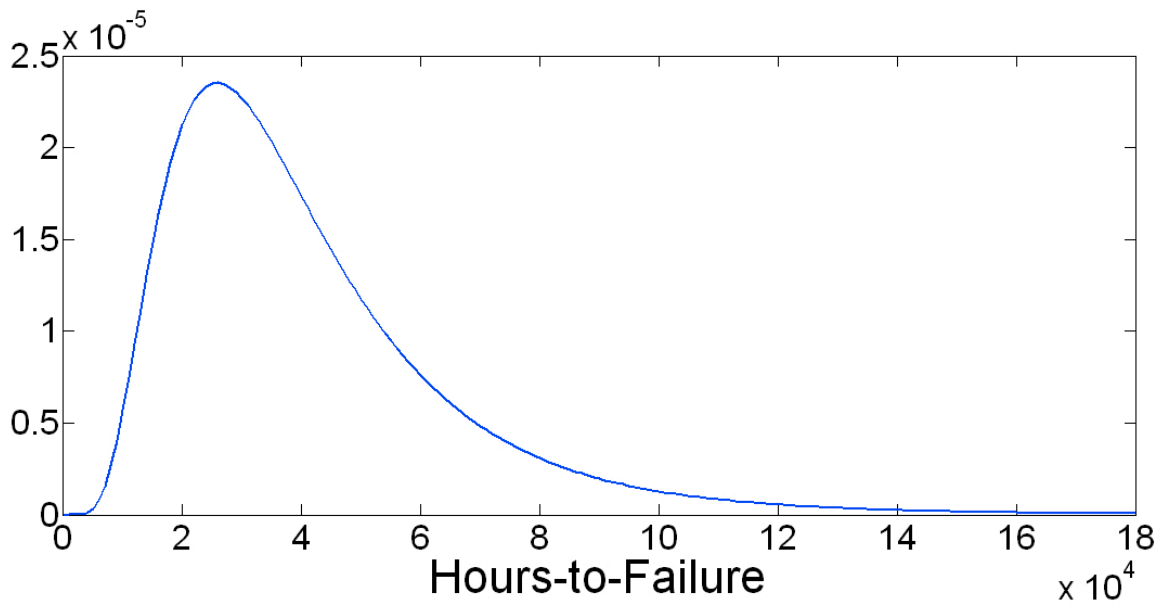


Figure 29. Hours-to-failure PDF

The sensitivity analysis using correlation coefficients is shown in table 16 for both usages (instructional and personal), for personal usage only in table 17, and for instructional usage only in table 18.

Higher correlation coefficients indicate more importance. The results show all variables except sink rate are significant. For personal usage, the gust is more significant relative to maneuver, whereas for instructional usage the reverse is true.

Table 16. Correlation analysis: personal and instructional usage

	Flights-to-Failure	Flight Length	Flight Speed	Sink Rate	Miner's Coefficient	Gust Factor	Maneuver Factor	Ground Stress	One-g Stress	P-S-N
Flights-to-Failure	1.0	-0.384	-0.307	-0.033	0.403	0.220	0.315	-0.279	0.281	0.380

Table 17. Correlation analysis: instructional usage

	Flights-to-Failure	Flight Length	Flight Speed	Sink Rate	Miner's Coefficient	Gust Factor	Maneuver Factor	Ground Stress	One-g Stress	P-S-N
Flights-to-Failure	1.0	-0.347	-0.255	-0.014	0.390	0.159	0.409	-0.172	0.172	0.366

Table 18. Correlation analysis: personal usage

	Flights-to-failure	Flight Length	Flight Speed	Sink Rate	Miner's Coefficient	Gust Factor	Maneuver Factor	Ground Stress	One-g Stress	P-S-N
Flights-to-Failure	1.0	-0.396	-0.196	-0.079	0.549	0.412	0.205	-0.286	0.286	0.5241

2.3.2 Hours Mode

Using the methodology for which the user specifies a number of flying hours for each usage, the second analysis was conducted to calculate the probability of crack initiation if the aircraft is flown for another 1,000 and 2,000 hours under personal usage, in addition to the 10,800 instructional and 2,000 in personal usage already flown. The main advantage of this analysis is to estimate the risk of an airplane flying any number of additional hours from its current condition. The data used for this analysis is the same as the damage mode example (see table 14).

The distribution of accumulated damage and Miner's damage coefficient are presented in figure 30. The results from the analysis showed an increment in the mean damage of approximately 7.8% from flying an additional 1000 hours and approximately 15.6% from flying an additional 2000 hours. The damage increment is linear because the flight conditions did not change between 1000 and 2000 hours. Table 19 shows the change in the POF for each of the three runs, showing an increment of the POF when the number of flying hours increases, as expected.

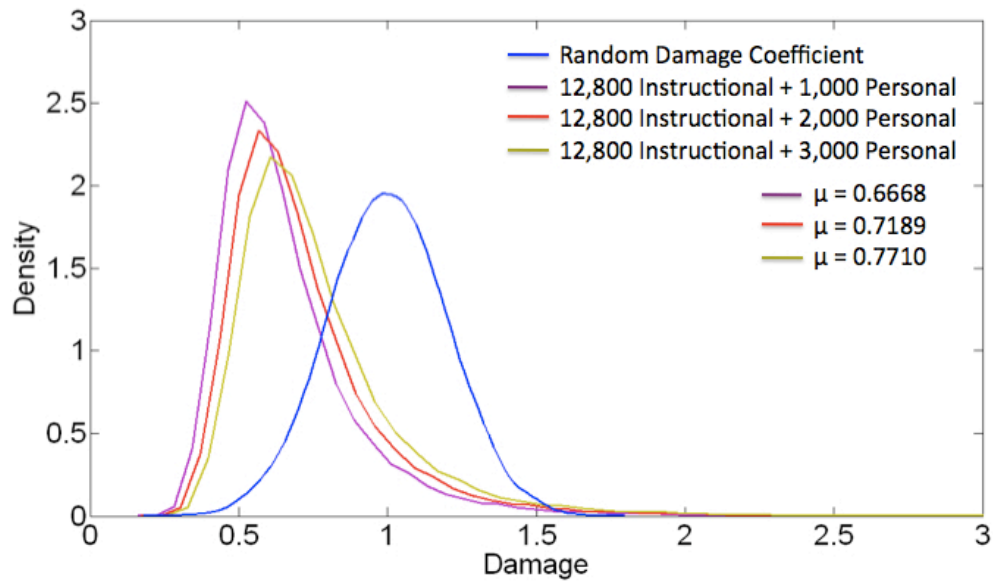


Figure 30. Mean damage results

Table 19. POF results

Current Condition 10,800 hours in instructional usage and 2,000 hours in personal usage	0.1209
10,800 hours in instructional usage, 2,000 hours in personal usage, and an additional 1,000 in personal usage	0.1576
10,800 hours in instructional usage, 2,000 hours in personal usage, and an additional 2,000 in personal usage	0.1995

3. CONCLUSIONS

Probabilistic fatigue evaluation of General Aviation aircraft is vital to provide important insight into the severity or criticality of a potential structural issue. For this reason, a probabilistic risk assessment methodology and computer software were developed so FAA engineers can perform a risk assessment of a structural issue. Because of significant airplane-to-airplane and flight-to-flight variations, probability density functions of the critical variables were investigated and developed.

The methodology and software were demonstrated on two different structural risk assessment examples.

4. REFERENCES

1. Reyer W. M. (2006). *Probability basis of safe-life evaluation in small airplanes*. Paper presented at the Aging Aircraft Conference, Atlanta, GA. Retrieved from http://www.slideshare.net/Yo_Creo/probability-basis-of-safe-life-evaluation-in-small-airplanes-by-w-michael-reyer
2. Raju, K. S., Smith, K. S., Caido, F., Gomez, C., & Shiao, M. (2009). Fatigue behavior of fastener joints. *SAE International Journal of Aerospace*, 1(1), 675–684.
3. Raju, K. S., Smith, B. L., Caido, F., Gomez, C., Shiao, M., & Nuss, M. (2010). Fatigue-based severity factors for shear-loaded fasteners. *AIAA Journal of Aircraft*, 47(1), 181–191.
4. FAA Report. (1973). Fatigue Evaluation of Wing and Associated Structure on Small Airplanes. (AFS120-73-2).
5. FAA Report. (2005). Fatigue Fail-Safe, and Damage Tolerance Evaluation of Metallic Structure for Normal, Utility, Acrobatic, and Commuter Category Airplanes. (AC 23-13A).
6. Hamby, D. M. (1995). A Comparison of Sensitivity Analysis Techniques. *Environmental Monitoring and Assessment*, 68(2), 195–204.
7. Ocampo, J. D., Acosta, C. A., & Millwater, H., *High performance computing implementation on a risk assessment problem*. Paper presented at the 48th AIAA Aerospace Sciences Meeting, Orlando, FL. Retrieved from <http://www.enu.kz/repository/2010/AIAA-2010-181.pdf>.
8. Singh, G., Acosta, C.A., Ocampo, J., & Millwater, H., *Distributed computing for probabilistic structural integrity analysis of aircraft structures*. Paper presented at the 51st AIAA/ASME/ASCE/AHS/ASC Structures, Structural Dynamics, and Materials Conference, Orlando, FL. Retrieved from arc.aiaa.org/doi/pdf/10.2514/6.2010-2848.
9. FAA Report. (1993). General Aviation Aircraft—Normal Acceleration Data Analysis and Collection Project. (DOT/FAA/CT-91/20).
10. United States Department of Commerce. (1964). *Handbook of Mathematical Functions*. Washington, D. C: U. S. Government Printing Office.
11. ASTM E739-91 (Reapproved 1998), “Statistical Analysis of Linear or Linearized Stress-Life (S-N) and Strain-Life (e-N) Fatigue Data” ASTM International, West Conshohocken, PA, 1998, DOI: 10.1520/E0739-10, www.astm.org.
12. Jarfall, L. (1972). Optimum Design of Joints: The Stress Severity Factor Concept. In J.Y. Mann and I.S. Milligan (Eds.) *Aircraft Fatigue, Design, Operational and Economic Aspects*. (337–380). Pergamon, Australia, Pergamon Press Australia.

13. Niu, C.Y. (2006). *Airframe Structural Design*. Granada Hills, CA: ADASO/ADASTRA Engineering Center.